Hadron-Hadron interactions from $N_f = 2 + 1 + 1$ lattice QCD: $I = 3/2$ πK scattering length

C. Helmes,[1,*] C. Jost,[1] B. Knippschild,[1] B. Kostrzewa,[1] L. Liu,[2] F. Pittler,[1] C. Urbach,[1] and M. Werner[1]

(ETM Collaboration)

[1]*Helmholtz Institut für Strahlen- und Kernphysik, University of Bonn, 53115 Bonn, Germany*
[2]*Institute of Modern Physics, Chinese Academy of Sciences, 730000 Lanzhou, China*

In this paper, we report on results for the s-wave scattering length of the π-K system in the $I = 3/2$ channel from $N_f = 2 + 1 + 1$ lattice QCD. The calculation is based on gauge configurations generated by the European Twisted Mass Collaboration with pion masses ranging from about 230 to 450 MeV at three values of the lattice spacing. Our main result reads $M_\pi a_0^{3/2,\mathrm{phys}} = -0.059(2)$. Using chiral perturbation theory we are also able to estimate $M_\pi a_0^{1/2,\mathrm{phys}} = 0.163(3)$. The error includes statistical and systematic uncertainties, and for the latter in particular errors from the extrapolation to the physical point.

I. INTRODUCTION

For understanding the strong interaction sector of the standard model (SM), it is not sufficient to compute masses of stable particles. Gaining insight into interactions of two or more hadrons and resonances is a must. Due to the nonperturbative nature of low-energy quantum chromodynamics (QCD), computations of interaction properties from lattice QCD are highly desirable. While ultimately the phase shift in a given partial wave is to be computed, also the scattering length is in many cases a useful quantity, in particular when the two-particle interaction is weak.

Due to the importance of chiral symmetry in QCD the investigation of systems with two pseudoscalar mesons is of particular interest. Here, chiral perturbation theory (ChPT) is able to provide a description of the pion mass dependence, and any nonperturbative computation, in turn, allows us to check this dependence. Naturally, ChPT works best for two pion systems, while convergence is unclear for pion-kaon or two kaon systems.

The two pion system is studied well experimentally, also in the different isospin channels. However, as soon as one or both pions are replaced by kaons, experimental results become sparse. On the other hand, this gap starts to be filled by lattice QCD calculations. For the pion-kaon system with isospin $I = 3/2$, there are by now a few lattice results available focusing on the scattering length [1–5]. The most recent computation in Ref. [4] uses one lattice at physical pion and kaon masses and lattice spacing $a \approx 0.114$ fm. For the sea and valence sector, they use $N_f = 2 + 1$ Möbius domain wall fermions and an Iwasaki gauge action. In Ref. [2], a systematic study of the elastic scattering lengths for the light pseudoscalar mesons was carried out with $N_f = 2 + 1$ $\mathcal{O}(a)$-improved Wilson quarks at pion masses ranging from 170 to 710 MeV and a lattice spacing $a \approx 0.09$ fm. Furthermore, Refs. [1,3] use $N_f = 2 + 1$ flavors on the MILC configurations with a rooted staggered sea quark action. Where Ref. [3] calculates the scattering length at a lattice spacing $a \approx 0.15$ fm, a slightly smaller lattice spacing $a \approx 0.125$ fm has been used in Ref. [1]. The pion masses in Ref. [1] range from 290 to 600 MeV, using domain wall valence quarks with a chiral extrapolation done in mixed-action chiral perturbation theory (MAChPT) [6,7]. The range of pion masses, 330 to 466 MeV, for the Asqtad improved staggered fermions of Ref. [3] is a bit smaller compared to Ref. [1]. In Ref. [5], the phase shifts and scattering lengths for π-K-scattering in $I = 3/2$ and $I = 1/2$ in the s-wave and the p-wave has been determined. The gauge action is a $N_f = 2$ tree-level improved Wilson-Clover action. The authors include the strange quark as a valence quark only which then corresponds to pion and kaon masses of $M_\pi = 266$ MeV and $M_K = 522$ MeV, respectively.

In this paper, we are going to present results for the s-wave scattering length of the pion-kaon system in the

*[*]helmes@hiskp.uni-bonn.de

elastic region with isospin $I = 3/2$. The investigation is based on gauge configurations produced by the European Twisted Mass Collaboration (ETMC) with $N_f = 2 + 1 + 1$ dynamical quark flavors [8]. In contrast to previous computations, we are able to investigate discretization effects and to extrapolate to physical quark masses owing to 11 ensembles with M_π ranging from 230 to 450 MeV distributed over three different lattice spacing values. We employ, in total, four different extrapolation methods to also estimate systematic uncertainties associated with our computation.

Finally, since this paper is the fourth in a series of publications [9–11] concerning elastic scattering of two pions in different channels and kaon-kaon with $I = 1$, we are able to compare results of two pseudoscalar mesons at maximal isospin involving different amounts of strangeness. The leading-order ChPT predictions for the dependence on the reduced mass divided by the relevant decay constant are identical for the three systems and differences appear only at NLO.

This paper is organized as follows: We first introduce the lattice details of our calculation. After the discussion of the analysis methods we present the main result, followed by a detailed discussion of the analysis details. We close with a discussion and summary. Technical details can be found in the Appendix.

II. LATTICE ACTION AND OPERATORS

A. Action

The lattice details for the investigation presented here are very similar to the ones we used to study the kaon-kaon scattering length [11]. We use $N_f = 2 + 1 + 1$ flavor lattice QCD ensembles generated by the ETM Collaboration, for which details can be found in Refs. [8,12,13]. The parameters relevant for this paper

TABLE I. The gauge ensembles used in this study. For the labeling of the ensembles, we adopted the notation in Ref. [13]. In addition to the relevant input parameters, we give the lattice volume and the number of evaluated configurations, N_{conf}.

Ensemble	β	$a\mu_\ell$	$a\mu_\sigma$	$a\mu_\delta$	$(L/a)^3 \times T/a$	N_{conf}
A30.32	1.90	0.0030	0.150	0.190	$32^3 \times 64$	259
A40.24	1.90	0.0040	0.150	0.190	$24^3 \times 48$	376
A40.32	1.90	0.0040	0.150	0.190	$32^3 \times 64$	246
A60.24	1.90	0.0060	0.150	0.190	$24^3 \times 48$	303
A80.24	1.90	0.0080	0.150	0.190	$24^3 \times 48$	300
A100.24	1.90	0.0100	0.150	0.190	$24^3 \times 48$	304
B35.32	1.95	0.0035	0.135	0.170	$32^3 \times 64$	241
B55.32	1.95	0.0055	0.135	0.170	$32^3 \times 64$	251
B85.24	1.95	0.0085	0.135	0.170	$32^3 \times 64$	288
D30.48	2.10	0.0030	0.120	0.1385	$48^3 \times 96$	364
D45.32sc	2.10	0.0045	0.0937	0.1077	$32^3 \times 64$	289

TABLE II. Values of the Sommer parameter r_0/a and the lattice spacing a at the three values of β. See Ref. [17] for details.

β	a [fm]	r_0/a
1.90	0.0885(36)	5.31(8)
1.95	0.0815(30)	5.77(6)
2.10	0.0619(18)	7.60(8)

are compiled in Table I: we give for each ensemble the inverse gauge coupling $\beta = 6/g_0^2$, the bare quark mass parameters μ_ℓ, μ_σ and μ_δ, the lattice volume and the number of configurations on which we estimated the relevant quantities.

The ensembles were generated using the Iwasaki gauge action and employ the $N_f = 2 + 1 + 1$ twisted mass fermion action [14–16]. For orientation, the β-values 1.90, 1.95 and 2.10 correspond to lattice spacing values of $a \sim 0.089$ fm, 0.082 fm, and 0.062 fm, respectively; see also Table II. The ensembles were generated at so-called maximal twist, which guarantees automatic $\mathcal{O}(a)$ improvement for almost all physical quantities [14]. The renormalized light quark mass m_ℓ is directly proportional to the light twisted quark mass via

$$m_\ell = \frac{1}{Z_P}\mu_\ell, \tag{1}$$

with Z_P the pseudoscalar renormalization constant. The relation of the bare parameters μ_σ and μ_δ to the renormalized charm and strange quark masses reads

$$m_{c,s} = \frac{1}{Z_P}\mu_\sigma \pm \frac{1}{Z_S}\mu_\delta, \tag{2}$$

with Z_S the nonsinglet scalar renormalization constant.

As noted in Refs. [13,17], the renormalized sea strange quark masses across the "A", "B" and "D" ensembles vary by up to about 20% and in a few cases differ from the physical strange quark mass to the same extent. For D30.48 and D45.32sc at the finest lattice spacing, the sea strange quark mass on the former ensemble overshoots the physical strange quark mass while it is consistent on the latter ensemble. In order to correct for these mistunings and to avoid the complicated flavor-parity mixing in the unitary nondegenerate strange-charm sector [8], we adopt a mixed action ansatz with so-called Osterwalder-Seiler (OS) [16] valence quarks, while keeping $\mathcal{O}(a)$ improvement intact. We denote the OS bare strange quark parameter with μ_s. It is related to the renormalized strange quark mass by

$$m_s = \frac{1}{Z_P}\mu_s. \tag{3}$$

For each ensemble, we investigate three values of μ_s which are compiled in Table III. More details on the mixed action approach can be found in Ref. [11].

TABLE III. Values of the bare strange quark mass $a\mu_s$ used for the three β-values. The lightest strange quark mass on the ensemble D30.48 is $a\mu_s = 0.0115$ instead of $a\mu_s = 0.013$.

β	1.90	1.95	2.10
$a\mu_s$	0.0185	0.0160	0.013/0.0115
	0.0225	0.0186	0.015
	0.0246	0.0210	0.018

As a smearing and contraction scheme we employ the stochastic Laplacian-Heaviside approach, described in Ref. [18]. Details of our parameter choices can be found in Refs. [9,11].

B. Lattice operators and correlation functions

For reasons that will become clear later, we need to estimate the masses of the pion, the kaon and the η meson on our ensembles. The masses for the pion and kaon are obtained from the large Euclidean time dependence of two point functions of the form

$$C_X(t - t') = \langle \mathcal{O}(X)(t)\mathcal{O}(X)^\dagger(t')\rangle, \qquad (4)$$

where $X \in \{\pi, K\}$. The operators for the charged pion and kaon projected to zero momentum read

$$\mathcal{O}(X)(t) = \sum_\mathbf{x} O_X(\mathbf{x}, t) \qquad (5)$$

with

$$O_\pi(\mathbf{x}, t) = i\bar{d}(\mathbf{x}, t)\gamma_5 u(\mathbf{x}, t), \qquad (6)$$

$$O_K(\mathbf{x}, t) = i\bar{s}(\mathbf{x}, t)\gamma_5 u(\mathbf{x}, t). \qquad (7)$$

For the η (and η') meson, we use the two operators

$$O_\ell(\mathbf{x}, t) = \frac{i}{\sqrt{2}}(\bar{u}(\mathbf{x}, t)\gamma_5 u(\mathbf{x}, t) + \bar{d}(\mathbf{x}, t)\gamma_5 d(\mathbf{x}, t)), \qquad (8)$$

$$O_s(\mathbf{x}, t) = i\bar{s}(\mathbf{x}, t)\gamma_5 s(\mathbf{x}, t). \qquad (9)$$

From these we build a two-by-two correlator matrix by taking the disconnected diagrams into account. The η (principal) correlator is determined by solving a generalized eigenvalue problem as described in detail in Ref. [19]. A complete discussion of the analysis of the η (and η') meson is beyond the scope of this paper and the full analysis will be presented in a future publication [20]. In addition to the aforementioned meson masses, we also need to estimate the energy $E_{\pi K}$ of the interacting pion-kaon two particle system. For the case of maximal isospin, i.e., $I = 3/2$, the corresponding two particle operator reads

$$\mathcal{O}(\pi K)(t) = -\sum_{\mathbf{x}, \mathbf{x}'} \bar{d}(\mathbf{x}, t)\gamma_5 u(\mathbf{x}, t)\bar{s}(\mathbf{x}', t)\gamma_5 u(\mathbf{x}', t). \quad (10)$$

It is used to construct the two-particle correlation function

$$C_{\pi K}(t - t') = \langle \mathcal{O}(\pi K)(t)\mathcal{O}(\pi K)^\dagger(t')\rangle. \qquad (11)$$

$E_{\pi K}$ can then be determined from the large Euclidean time dependence of $C_{\pi K}$.

III. ANALYSIS METHODS

We focus in this work on pion-kaon scattering in the elastic region. For small enough squared scattering momentum p^2, one can perform the effective range expansion for partial wave ℓ

$$p^{2\ell+1}\cot(\delta_\ell) = -\frac{1}{a_\ell} + \mathcal{O}(p^2) \qquad (12)$$

with phase shift δ_ℓ and scattering length a_ℓ. For the pion-kaon system, it is, to a very good approximation, sufficient to study the s-wave, i.e., $\ell = 0$.

In lattice QCD, the phase shift or the scattering length can only be computed from finite volume induced energy shifts. The relevant energy shift here is given by

$$\delta E = E_{\pi K} - M_\pi - M_K. \qquad (13)$$

Using again the effective range expansion, one arrives at the Lüscher formula [21]

$$\delta E = -\frac{2\pi a_0}{\mu_{\pi K} L^3}\left(1 + c_1\frac{a_0}{L} + c_2\frac{a_0^2}{L^2}\right) + \mathcal{O}(L^{-6}) \quad (14)$$

relating δE directly to the scattering length a_0, the reduced mass of the pion-kaon system,

$$\mu_{\pi K} = \frac{M_\pi M_K}{M_\pi + M_K}, \qquad (15)$$

and the spatial extent of the finite volume L. The coefficients read [21]

$$c_1 = -2.837297, \qquad c_2 = 6.375183.$$

Given δE, $\mu_{\pi K}$ and L, Lüscher's formula allows one to determine the scattering length a_0 by solving Eq. (14) for a_0. In what follows, we will describe how we extract δE and the other relevant bare quantities from correlation functions. Then we will give details on our approach to interpolate or extrapolate the results to physical conditions and the investigation of discretization artifacts.

In order to gain some understanding of systematic uncertainties, we perform the analysis in two different ways once the bare data has been extracted. Combined

chiral and continuum extrapolations are performed at fixed strange quark mass using next-to-leading-order ChPT (NLO ChPT) and a variant thereof referred to as the Γ method, as described in Ref. [1]. In addition, we explore possible discretization effects of $\mathcal{O}(a^2)$.

A. Physical inputs

For the analysis presented below, we require physical inputs for the pion, the kaon and η-meson masses as well as the pion decay constant. To this end, we employ the values in the isospin symmetric limit, $\bar{M}_\pi$ and $\bar{M}_K$, as determined in chiral perturbation theory [22] and given in Ref. [23] as

$$\bar{M}_\pi = 134.8(3) \text{ MeV},$$
$$\bar{M}_K = 494.2(3) \text{ MeV}. \tag{16}$$

For the η meson mass, we use the average obtained by the Particle Data Group [24]:

$$\bar{M}_\eta = 547.86(2) \text{ MeV}. \tag{17}$$

For the decay constant, we use the phenomenological average determined by the Particle Data Group given in Ref. [25] as

$$f_{\pi^-}^{(\text{PDG})} = 130.50(13) \text{ MeV}. \tag{18}$$

As an intermediate lattice scale, we employ the Sommer parameter r_0 [26]. It was determined in Ref. [17] from the ensembles we use here to be

$$r_0 = 0.474(11) \text{ fm}. \tag{19}$$

In the parts of the analysis which require r_0, we use parametric bootstrap samples with central value and width given in Eq. (19). Where r_0/a values enter as fit parameters, we constrain the corresponding fit parameters using Gaussian priors in the augmented χ^2 function given as

$$\chi^2_{\text{aug}} = \chi^2 + \sum_\beta \left(\frac{(r_0/a)(\beta) - P_r(\beta)}{\Delta r_0/a(\beta)} \right)^2. \tag{20}$$

B. Energy values from correlation functions

The energies of the two point correlation functions as given in Eq. (4) are extracted from fits of the form

$$C_X(t) = A_0^2(e^{-E_X t} + e^{-E_X(T-t)}), \tag{21}$$

to the data. While for M_K and M_π the signal extends up to $T/2$, for the η we have to face more noise. We deal with this by applying the excited state subtraction method used and described in Refs. [19,27].

In the determination of the energy shift δE, the total energy $E_{\pi K}$ of the interacting π-K system must be computed. However, in the spectral decomposition of the two-particle correlation function, unwanted time dependent contributions, so-called thermal pollution, appear. Taking into account that our π-K correlation function is symmetric around the $T/2$ point, the leading contributions in the spectral decomposition can be cast into the form

$$C_{\pi K}(t) = A_0^2(e^{-E_{\pi K} t} + e^{-E_{\pi K}(T-t)})$$
$$+ A_1(e^{-E_\pi T} e^{(E_\pi - E_K)t} + e^{-E_K T} e^{(E_K - E_\pi)t}), \tag{22}$$

where

$$A_0^2 = \langle \Omega | \pi^+ K^+ | \pi K \rangle \langle \pi K | (\pi^+ K^+)^\dagger | \Omega \rangle, \tag{23}$$

is the overlap of the two particle operator $\mathcal{O}(\pi K)$ of Eq. (10) with the vacuum Ω and only the first line corresponds to the energy level we are interested in. However, at finite T-values, the second contribution might be sizable, in particular at times close to $T/2$. Moreover, the thermal pollution cannot be separated easily from the signal we are interested in. We have studied two different methods, labeled **E1** and **E2**, to extract $E_{\pi K}$ from $C_{\pi K}(t)$, where **E1** has already been discussed in Ref. [28].

  (i) **E1**: weighting and shifting: To render one of the polluting terms in Eq. (22) time independent, the correlation function first gets weighted by a factor $\exp((E_K - E_\pi)t)$. We chose this factor, because $\exp(-E_\pi T)$ is significantly larger than $\exp(-E_K T)$. The resulting constant term can then be removed by the shifting procedure, which thus replaces $C_{\pi K}(t)$ by

$$C_{\pi K}^w(t) = e^{(E_K - E_\pi)t} C_{\pi K}(t),$$
$$\tilde{C}_{\pi K}^w(t) = C_{\pi K}^w(t) - C_{\pi K}^w(t + \delta t), \tag{24}$$

where δt is a fixed number of time slices.

Subsequently, we multiply $\tilde{C}_{\pi K}^w(t)$ by $\exp(-(E_K - E_\pi)t)$, which (mostly) recovers the original time dependence in the contribution of interest

$$C_{\pi K}^{\text{E1}}(t) = e^{-(E_K - E_\pi)t} \tilde{C}_{\pi K}^w(t). \tag{25}$$

We now extract the total energy of the π-K system, $E_{\pi K}$. To this end, we apply Eqs. (24) and (25) to the data at hand and then fit

$$C_{\pi K}^{\text{E1}}(t) = A_0^2(e^{-E_{\pi K} t} + e^{-E_{\pi K}(T-t)}$$
$$- e^{(E_K - E_\pi)\delta t}(e^{-E_{\pi K}(t+\delta t)} + e^{-E_{\pi K}(T-(t+\delta t))}))$$
$$+ \tilde{A}_1 e^{(E_K - E_\pi)t}. \tag{26}$$

Note that in contrast to Ref. [28], where correlator matrices with various sources of thermal pollution are

considered, we are able to take $\tilde{A}_1$ as an additional fit parameter in order to account for this subleading term.

(ii) **E2**: dividing out the pollution: To improve on method **E1**, we assume that the decomposition given in Eq. (22) allows one to neglect any further thermal pollution. This leads to dividing out the time dependent part

$$p(t) = e^{(E_K - E_\pi)t} e^{-E_K T} + e^{-(E_K - E_\pi)t} e^{-E_\pi T}, \quad (27)$$

explicitly. With

$$C'_{\pi K}(t) = \frac{C_{\pi K}(t)}{p(t)} \quad (28)$$

we then proceed to calculate

$$\tilde{C}_{\pi K}(t) = C'_{\pi K}(t) - C'_{\pi K}(t + \delta t), \quad (29)$$

$$C^{E2}_{\pi K}(t) = p(t)\tilde{C}_{\pi K}(t), \quad (30)$$

from which we extract $E_{\pi K}$ through fitting

$$C^{E2}_{\pi K}(t) = A_0^2 \left(e^{-E_{\pi K}t} + e^{-E_{\pi K}(T-t)} - \frac{p(t)}{p(t+1)} \right.$$
$$\left. \cdot \left(e^{-E_{\pi K}(t+1)} + e^{-E_{\pi K}(T-(t+1))} \right) \right). \quad (31)$$

We remark that for both methods **E1** and **E2** the energies E_π and E_K, i.e., M_π and M_K for zero momentum, are required as an input. They are determined from the corresponding two-point correlation functions. Please note that in method **E2** we need to fit one amplitude, A_0, while method **E1** requires to take care of two amplitudes, A_0 and $\tilde{A}_1$. For the error analysis, bootstrap samples are used to fully preserve all correlations.

After solving Eq. (14) for a_0 up to $\mathcal{O}(L^{-5})$ on every ensemble for each strange quark mass of Table III, we have three parameters in which we want to extra- or interpolate: the lattice spacing a, the strange quark mass m_s and the light quark mass m_ℓ. To evaluate a_0 at the physical point we follow a two-step procedure. We first fix the strange quark mass to its physical value and subsequently perform a combined chiral and continuum extrapolation, investigating different possible types of discretization artifacts.

C. Fixing the strange quark mass

In order to fix the strange quark mass, we adopt the following procedure: we match the quantity

$$M_s^2 = M_K^2 - 0.5M_\pi^2, \quad (32)$$

which is proportional to the strange quark mass at the leading order of ChPT, to its physical value

$$(M_s^{\text{phys}})^2 = \bar{M}_K^2 - 0.5\bar{M}_\pi^2, \quad (33)$$

using our determinations of M_K^2 at three valence strange quark masses on a per-ensemble basis. For each ensemble, we then interpolate all valence strange quark mass dependent observables, i.e., $\mu_{\pi K} a_0^{3/2}$, M_K, M_η and $\mu_{\pi K}$, in M_s^2 to this reference value.

D. Chiral extrapolation

With the strange quark mass fixed, the extrapolation to the physical point can be carried out using ChPT. The first NLO calculation of the scattering amplitude and scattering lengths was done in Ref. [29]. From the continuum ChPT formulae for the isospin even (odd) scattering lengths a^+ (a^-) in Ref. [30], the NLO ChPT formulae for $\mu_{\pi K} a_0^I$, $I \in \{1/2, 3/2\}$, can be derived as sketched in Appendix A, giving

$$\mu_{\pi K} a_0^{3/2} = \frac{\mu_{\pi K}^2}{4\pi f_\pi^2} \left[\frac{32 M_\pi M_K}{f_\pi^2} L_{\pi K}(\Lambda_\chi) - 1 - \frac{16 M_\pi^2}{f_\pi^2} L_5(\Lambda_\chi) \right.$$
$$\left. + \frac{1}{16\pi^2 f_\pi^2} \chi^{3/2}_{\text{NLO}}(\Lambda_\chi, M_\pi, M_K, M_\eta) \right] + c \cdot f(a^2).$$
$$(34)$$

Equation (34) depends on the masses of the pion and the kaon, their reduced mass as defined in Eq. (15), the η mass and the pion decay constant. In addition, the equation depends on the low-energy constants (LECs) L_5 and $L_{\pi K}$ while $\chi^{3/2}_{\text{NLO}}$ is a known function; see Appendix A 2.

We express Eq. (34) in terms of the meson masses and decay constants as they are determined on the lattice, which has the benefit that their ratios can be computed with high statistical precision without the need for explicit factors of the lattice scale. Hence we fit all lattice data simultaneously. Formally, we fix the scale-dependent LECs at the renormalization scale $\Lambda_\chi = f_{\pi^-}^{(\text{PDG})}$. However, in practice we employ $a\Lambda_\chi = af_\pi(\beta, \mu_\ell)/K_{f_\pi}^{\text{FSE}}$ in all chiral logarithms, where the values for the finite-size correction factor $K_{f_\pi}^{\text{FSE}}$ are given in Sec. V B. Doing so should only induce higher-order corrections in the chiral expansion.

Automatic $\mathcal{O}(a)$ improvement of Wilson twisted mass fermions at maximal twist guarantees that the leading lattice artifacts are of $\mathcal{O}(a^2)$ or better. For instance, for the $I = 2$ $\pi\pi$ s-wave scattering length, discretization effects start only at $\mathcal{O}(a^2 M_\pi^2)$ [31]. A corresponding theoretical result for πK is missing so far. However, our numerical data suggest that also for πK lattice artifacts are very small. Still, we include a term $c \cdot f(a^2)$ accounting for possible discretization effects, with fit parameter c and $f(a^2)$ either equal to a^2/r_0^2 or to $a^2 M_X^2$, with M_X^2 one of the masses or mass combinations M_π^2, M_K^2, $M_K^2 + 0.5M_\pi^2$, $\mu_{\pi K}^2$. In the following analysis, we will include the term $c \cdot f(a^2)$ into our fit for every choice of $f(a^2)$ and thus investigate a possible dependence of our data on the lattice spacing.

To summarize, our fit parameters are the LECs L_5 and $L_{\pi K}$, and c, where $L_{\pi K}$ is the combination of renormalized LECs

$$L_{\pi K} = 2L_1 + 2L_2 + L_3 - 2L_4 - \frac{L_5}{2} + 2L_6 + L_8. \quad (35)$$

Let us mention already here that the fits to the data described in the next section turn out to be not sensitive to L_5. Therefore, we include it as a prior in the fit with the value taken from Ref. [23]. In a slight abuse of the language, we will denote this extrapolation method as NLO ChPT.

E. Extrapolations using the Γ method at fixed m_s

Next, we describe an alternative way to extrapolate our data, first applied in Ref. [1]. In what follows, we just shortly introduce the derivation of the fit formula and refer to Appendix A 2 for a more detailed discussion. To derive the relevant formulae we first plug the expressions for a^+ and a^- (cf. Appendix A 2) into Eq. (A4) and reorder such that LECs appear on one side of the equation. The result reads

$$L_5 - 2\frac{M_K}{M_\pi}L_{\pi K} = \frac{f_\pi^2}{16M_\pi^2}\left(\frac{4\pi f_\pi^2}{\mu_{\pi K}^2}[\mu_{\pi K}a_0^{3/2}] + 1\right.$$
$$+ \chi_{\mathrm{NLO}}^-(\Lambda_\chi, M_\pi, M_K, M_\eta)$$
$$\left. - 2\frac{M_K M_\pi}{f_\pi^2}\chi_{\mathrm{NLO}}^+(\Lambda_\chi, M_\pi, M_K, M_\eta)\right), \quad (36)$$

with $\chi_{\mathrm{NLO}}^\pm(\Lambda_\chi, M_\pi, M_K, M_\eta)$ given in Appendix A 2. We label the right-hand side of Eq. (36) $\Gamma(M_\pi/f_\pi, M_K/f_\pi)$ which comprises only measurable quantities:

$$\Gamma\left(\frac{M_\pi}{f_\pi}, \frac{M_K}{f_\pi}\right) = L_5 - 2\frac{M_K}{M_\pi}L_{\pi K}. \quad (37)$$

Having calculated $\Gamma(M_\pi/f_\pi, M_K/f_\pi)$ using the interpolated data of $\mu_{\pi K}a_0^{3/2}$, M_K, M_η and $\mu_{\pi K}$, and the data of M_π and f_π we fit Eq. (37) via L_5 and $L_{\pi K}$ to the data obtained in this way. Please note that also Γ is still dimensionless which enables a fit to all lattice data simultaneously. Given L_5 and $L_{\pi K}$ from the fit one can compute $\mu_{\pi K}a_0^{3/2}$ at the physical point using Eq. (34). Again, it turns out we are not sensitive to L_5 in our fits. Therefore, we use a prior as discussed before. This extrapolation method we denote as Γ method.

IV. RESULTS

In this section, we present our main result for $\mu_{\pi K}a_0^{3/2}$ extrapolated to the physical point.

We use two thermal state pollution removal methods, **E1** and **E2**, for $E_{\pi K}$. Next, we employ the two (related) ChPT extrapolations, Γ method and NLO ChPT, as discussed

TABLE IV. Fit ranges used for extrapolations Γ and NLO ChPT. The index column refers to Fig. 1.

Method	Index	Begin	End
Γ	1	1.2	2.0
	2	1.4	2.0
	3	1.5	2.0
NLO	1	1.2	1.6
	2	1.2	1.41
	3	1.2	1.35

before. For reasons that will be detailed in Sec. V D 1, we state the NLO ChPT results with $c = 0$. For each of the two ChPT extrapolation methods, we use three fit ranges as compiled in Table IV. Hence, we have 12 estimates for each quantity at the physical point available, which we use to estimate systematic uncertainties. We remark that the fit for the Γ method is in terms of M_K/M_π and for NLO ChPT in terms of $\mu_{\pi K}/f_\pi$. Thus, we vary the fit range at the lower end for the Γ method and at the upper end for NLO ChPT.

For $\mu_{\pi K}a_0^{3/2}$, the 12 estimates are shown in Fig. 1. The final result is obtained as the weighted average over all of these, as shown in the figure as the horizontal bold line. The weight is computed according to

$$w = \frac{(1 - 2 \cdot |p - 1/2|)^2}{\Delta^2} \quad (38)$$

with p the p-value of the corresponding ChPT fit and Δ the statistical uncertainty obtained from the fit.

The statistical uncertainty of the final results is determined from the bootstrap procedure. For $\mu_{\pi K}a_0^{3/2}$, this is shown in Fig. 1 as the inner error band. In addition, we determine three systematic uncertainties: The first is obtained from the difference between using only **E1** or only **E2** results. The second from the difference between
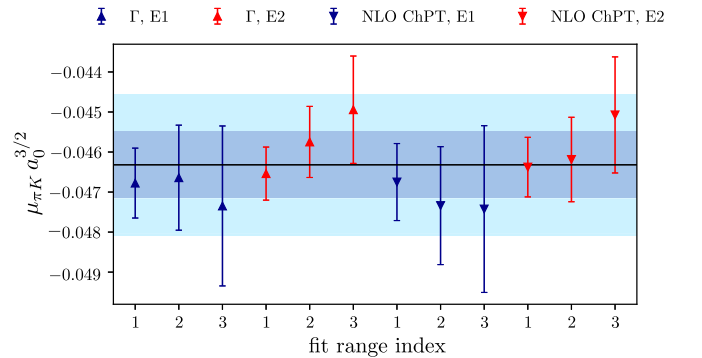
FIG. 1. Comparison of values for $\mu_{\pi K}a_0^{3/2}$ at the physical point obtained with the different methods used in this paper. The fit ranges decrease with increasing index as described in Table IV. The inner error band represents the statistical error only, while the outer error band represents the statistical and systematic errors added in quadrature.

TABLE V. Fit results of the chiral exptrapolation using the Γ method. The fits shown in Fig. 5 correspond to the largest fit range in the table.

Removal	Fit range	p-value	$L_{\pi K} \times 10^3$	$\mu_{\pi K} a_0^{3/2} \times 10^2$
E1	0.0 to 2.0	0.8	3.7(2)	$-4.68(9)$
	1.4 to 2.0	0.7	3.7(2)	$-4.7(1)$
	1.5 to 2.0	0.6	3.6(3)	$-4.7(2)$
E2	0.0 to 2.0	0.3	3.7(1)	$-4.65(7)$
	1.4 to 2.0	0.5	3.8(2)	$-4.57(9)$
	1.5 to 2.0	0.4	4.0(2)	$-4.5(1)$

using only the Γ method or only NLO ChPT. Finally, we use the maximal difference of the weighted average to the 12 estimates as a systematic uncertainty coming from the choice of fit ranges.

The results of all twelve fits can be found in Table V for the Γ method and Table VII for NLO ChPT fits. The fit range indices used in Fig. 1 are resolved in Table IV. The results for all approaches after averaging over the fit ranges are listed in Table IX, in Appendix B.

With this procedure and all errors added in quadrature we quote

$$\mu_{\pi K} a_0^{3/2,\text{phys}} = -0.0463(17), \qquad L_{\pi K} = 0.0038(3). \quad (39)$$

This translates to

$$M_\pi a_0^{3/2,\text{phys}} = -0.059(2), \qquad M_\pi a_0^{1/2,\text{phys}} = 0.163(3) \quad (40)$$

as our final results. The error budget is compiled in Table VIII. While the dominating contribution to the error for both $\mu_{\pi K} a_0^{3/2}$ and $L_{\pi K}$ summed in quadrature is coming from the fit range and the statistical uncertainty, also the choice of the thermal state removal method contributes significantly. The contribution from the different chiral extrapolation methods is negligible. If the errors were added (not in quadrature), the total error would become a factor ∼1.7 larger.

We remark that these results have been obtained with L_5 as an input, because the fits are not sufficiently sensitive to determine L_5 directly. We use the most recent determination from a $N_f = 2 + 1 + 1$ lattice calculation by HPQCD [23], which is extrapolated to the continuum limit. At our renormalization scale, it reads

$$L_5 = 5.4(3) \times 10^{-3}. \quad (41)$$

V. ANALYSIS DETAILS AND DISCUSSION

A. Error analysis, thermal pollution and choice of fit ranges

The error analysis is performed using the stationary blocked bootstrap procedure [32]. In order to determine an appropriate average block length, we compute the integrated autocorrelation time τ_{int} for the correlation functions $C_X(t)$ at all source-sink separations, with X being π, K, η or πK. In the case of πK, $C_X(t)$ is of course first suitably transformed for the extraction of the interaction energy as discussed in Sec. III B. The computation of τ_{int} is detailed in Ref. [33]. The average block length is then chosen to be the ceiling of the maximum integrated autocorrelation time observed over all correlation functions at all source-sink separations

$$b = \lceil \max_{X,t}(\tau_{\text{int}}^{(X,t)}) \rceil$$

on a per-ensemble basis. We have confirmed explicitly that this method produces a block length at which the estimate of the statistical error plateaus and are thus confident that we properly take into account the effect of autocorrelations on our quoted statistical errors. Using the so-determined block length on a per-ensemble basis, we generate $N = 1500$ samples from which we estimate statistical errors throughout our analysis.

As discussed in Sec. III B, we employ methods **E1** and **E2** to remove unwanted thermal pollution from the πK two particle correlation function. Both methods allow us to describe the data rather well, but the choice of best fit range depends on the method used to remove the thermal pollution. This, in turn, affects the value of the extracted $E_{\pi K}$ and, subsequently, the value of $\mu_{\pi K} a_0^{3/2}$ obtained from the energy difference.

To demonstrate the quality of our fits, we look at the ratio

$$\frac{C_{\pi K}^{[\text{E1,E2}]}(t)}{f^{[\text{E1,E2}]}(t)}, \quad (42)$$

where $C^{[\text{E1,E2}]}$ are defined in Eqs. (25) and (30), respectively, and the fit functions $f^{[\text{E1,E2}]}(t)$ are given in Eqs. (26) and (31), respectively. The ratio is shown in Fig. 2 for the two ensembles A40.24 and A40.32 for two fit ranges for which both methods describe the data well.

The choice of the fit ranges to determine energy levels is always difficult. In the past, we have used many fit ranges and weighted them according to their fit qualities [9,11]. However, this procedure relies on properly estimated variance-covariance matrices, which is notoriously difficult. For the pion-kaon correlation functions needed in this paper, we have observed several cases where the fit including the variance-covariance matrix did not properly describe the data after visual inspection. Therefore, we use fits here assuming independent data points with the correlation still taken into account by the bootstrap procedure.

As a consequence, we cannot apply the weighting procedure used in Refs. [9,11] any longer and have to choose fit ranges. The procedure is as follows: Due to exponential error growth of $C_{\pi K}$ we fix $t_f = T/2 - 4a$ and vary t_i, beginning from a region where excited states do not contribute significantly anymore. From these fits we choose

(a) Fit range: $[14, 20]$
$aE_{\pi K} = \{0.389(1)^{\text{E1}}, 0.389(1)^{\text{E2}}\}$

(b) Fit range: $[20, 28]$
$aE_{\pi K} = \{0.3793(6)^{\text{E1}}, 0.3789(5)^{\text{E2}}\}$
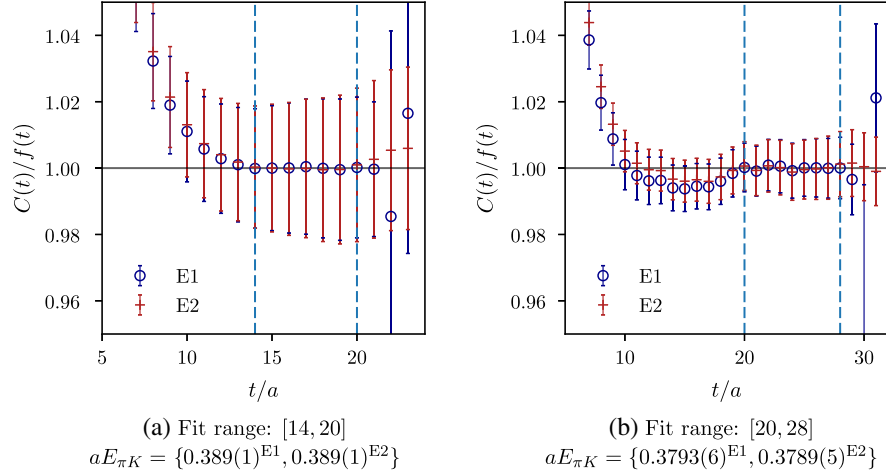
FIG. 2. Plot of Eq. (42) for ensembles A40.24 and A40.32 for the lightest strange quark mass for the fit ranges used for the analysis, comparing the quality of the data description by methods **E1** and **E2**.

one fit range where the ratio of Eq. (42) is best compatible with 1. The statistical error is calculated from the bootstrap samples as discussed before. We then estimate the systematic uncertainty from the remaining fit ranges. To this end, we determine the difference of the mean value to the upper and lower bound of values for $E_{\pi K}$. This procedure results in an asymmetric estimate of the systematic uncertainty of $E_{\pi K}$. The results are compiled in Table X, in Appendix B. Since C_K and C_π do not suffer from exponential error growth at late times we set $t_f = T/2$. Table VI gives an overview of our chosen values of t_i and t_f for all ensembles.

It is always difficult to include systematic uncertainties in the analysis chain. Since we see systematic uncertainties on extracted energies on the same level as the statistical one, we adopt the following procedure to include this uncertainty: Because $\mu_{\pi K} a_0^{3/2}$ is derived from $E_{\pi K}$, we chose to scale the statistical error for $\mu_{\pi K} a_0^{3/2}$ on each ensemble after the data have been interpolated in the strange quark mass. To this

end, we define a scaling factor s via the standard error ΔX and the average of the systematic uncertainties $\bar{Q}_X$ over the three strange quark masses for each ensemble,

$$s = \sqrt{\frac{(\Delta X)^2 + \bar{Q}_X^2}{(\Delta X)^2}}, \qquad (43)$$

where the average $\bar{Q}_X$ is the simple mean over the six systematic errors.

B. Meson masses, energy shift δE and scattering length $\mu_{\pi K} a_0^{3/2}$

In order to extract δE, we first determine M_K and M_π from fitting Eq. (21) to our data for $C_\pi(t)$ and $C_K(t)$. We then calculate the reduced mass $\mu_{\pi K}$ via Eq. (15) for all combinations of fit ranges. M_π, M_K and $\mu_{\pi K}$ are listed in Table XI, in Appendix B.

The two methods **E1** and **E2** give us two estimates of $E_{\pi K}$ as outlined in Sec. III B, from which we determine δE and hence the scattering length using Eq. (14). The values for $E_{\pi K}$ and δE are collected in Tables X, in Appendix B and XII, in Appendix B.

TABLE VI. Typical minimal and maximal values of the starting and end points of fit ranges for the Correlation functions under investigation.

Ensemble	aM_π		aM_K		$aE_{\pi K}$	
	t_i	t_f	t_i	t_f	t_i	t_f
A30.32	13	32	13	32	21	28
A40.24	11	24	11	24	14	20
A40.32	13	32	13	32	20	28
A60.24	11	24	11	24	16	20
A80.24	11	24	11	24	16	20
A100.24	11	24	11	24	15	20
B35.32	13	32	13	32	22	28
B55.32	13	32	13	32	19	28
B85.24	11	24	11	24	15	20
D45.32sc	14	32	14	32	22	28
D30.48	22	48	22	48	35	44

TABLE VII. Fit results for the NLO ChPT fit. The fits shown in Fig. 4 correspond to the largest fit range in the table.

Removal	Fit range	p-value	$L_{\pi K} \times 10^3$	$\mu_{\pi K} a_0^{3/2} \times 10^2$
E1	0.0 to 1.35	0.6	3.6(3)	$-4.7(2)$
	0.0 to 1.41	0.7	3.6(2)	$-4.7(1)$
	0.0 to 1.60	0.7	3.7(2)	$-4.7(1)$
E2	0.0 to 1.35	0.5	3.9(2)	$-4.5(1)$
	0.0 to 1.41	0.5	3.8(2)	$-4.6(1)$
	0.0 to 1.60	0.4	3.7(1)	$-4.64(7)$

TABLE VIII. Error budget for the final results of $\mu_{\pi K} a_0^{3/2}$ and $L_{\pi K}$.

	$\mu_{\pi K} a_0^{3/2} \times 10^5$	$L_{\pi K} \times 10^5$
Statistical	82 (28%)	15 (32%)
Fit range	139 (47%)	19 (41%)
E1 vs. **E2**	64 (22%)	12 (24%)
NLO ChPT vs. Γ	9 (3%)	1 (3%)
$\sum$	294 (100%)	47 (100%)
sqrt $\sum$ in quadrature	173	27

We introduce factors K_X^{FSE} for $X \in \{M_K, M_\pi, f_\pi\}$ to correct our lattice data for finite-size effects. They have already been calculated in Ref. [17] and are listed in Table XIII, in Appendix B. We apply these factors for e.g., M_π as

$$M_\pi^* = \frac{M_\pi}{K_{M_\pi}^{\mathrm{FSE}}}.$$

We correct every quantity of the set named above and drop the asterisk in what follows to improve legibility. For M_η, statistical uncertainties are too big to resolve finite volume effects; see also Ref. [34].

For the two methods **E1** and **E2**, we solve Eq. (14) for a_0 up to $\mathcal{O}(L^{-5})$ numerically. The values for a_0 and its product with the reduced mass, $\mu_{\pi K} a_0^{3/2}$ are collected in Table XIV, in Appendix B. Since the finite-size behavior of the scattering length is unknown, we do not apply finite-size corrections to the reduced mass appearing in $\mu_{\pi K} a_0^{3/2}$, either.

C. Strange quark mass fixing

Before we perform a combined continuum and chiral extrapolation, we interpolate all data to reference strange quark masses as discussed before. The data for the three

strange quark masses are strongly correlated because the same stochastic light perambulators were used for all light-strange observables. As a consequence, the variance-covariance matrix was sometimes not sufficiently well estimated such that its inverse was unreliable. As a result, we resort to performing these fits using uncorrelated χ^2 which results in best fit parameters which describe the data much better. It should be noted that all statistical covariance is still fully taken into account by the bootstrap procedure and our final statistical errors on all fit parameters are correctly estimated.

As an example, we show in Fig. 3 the interpolation of $\mu_{\pi K} a_0^{3/2}$ in $M_K^2 - 0.5 M_\pi^2$ for ensemble B55.32 comparing methods **E1** and **E2**. The large uncertainty in the interpolation variable stems mainly from the uncertainty in the scaling quantity r_0. Furthermore the errors of the three data points are highly correlated. The interpolation to the reference point is shown as a red diamond. In general, the strange quark mass dependence of $\mu_{\pi K} a_0^{3/2}$ is mild and stems mainly from the reduced mass $\mu_{\pi K}$. The values thus determined are compiled in Table XV, in Appendix B. They serve as input data for the subsequent chiral extrapolations.

D. Chiral extrapolations and discretization effects

Having interpolated all our lattice data to a fixed reference strange quark mass corresponding to the physical strange quark mass at leading chiral order, we will describe below the results and possible systematic errors in our chiral extrapolations.

1. Chiral perturbation theory at NLO

To investigate possible discretization effects we first let c in Eq. (34) vary freely and fit Eq. (34) for the different

(a) B55.32 for **E1**

(b) B55.32 for **E2**
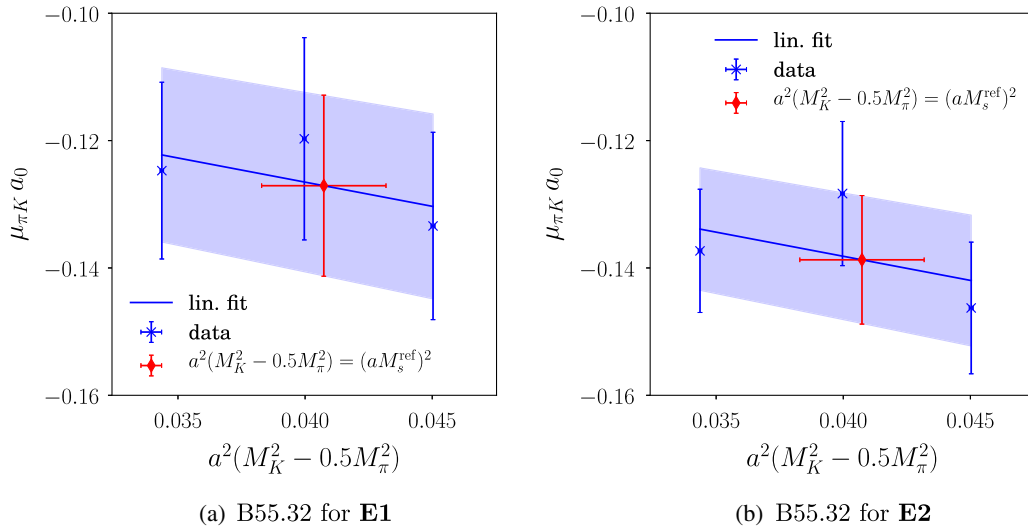
FIG. 3. Interpolations of $\mu_{\pi K} a_0^{3/2}$ for the two different methods **E1** and **E2**.

(a) **E1**:$\mu_{\pi K} a_0^{3/2}$ in terms of $\mu_{\pi K}/f_\pi$ together with LO ChPT formula.

(b) **E1**:Relative deviation between the measured and the fitted values of $\mu_{\pi K} a_0^{3/2}$.

(c) **E2**:$\mu_{\pi K} a_0^{3/2}$ in terms of $\mu_{\pi K}/f_\pi$ together with LO ChPT formula.

(d) **E2**:Relative deviation between the measured and the fitted values of $\mu_{\pi K} a_0^{3/2}$.
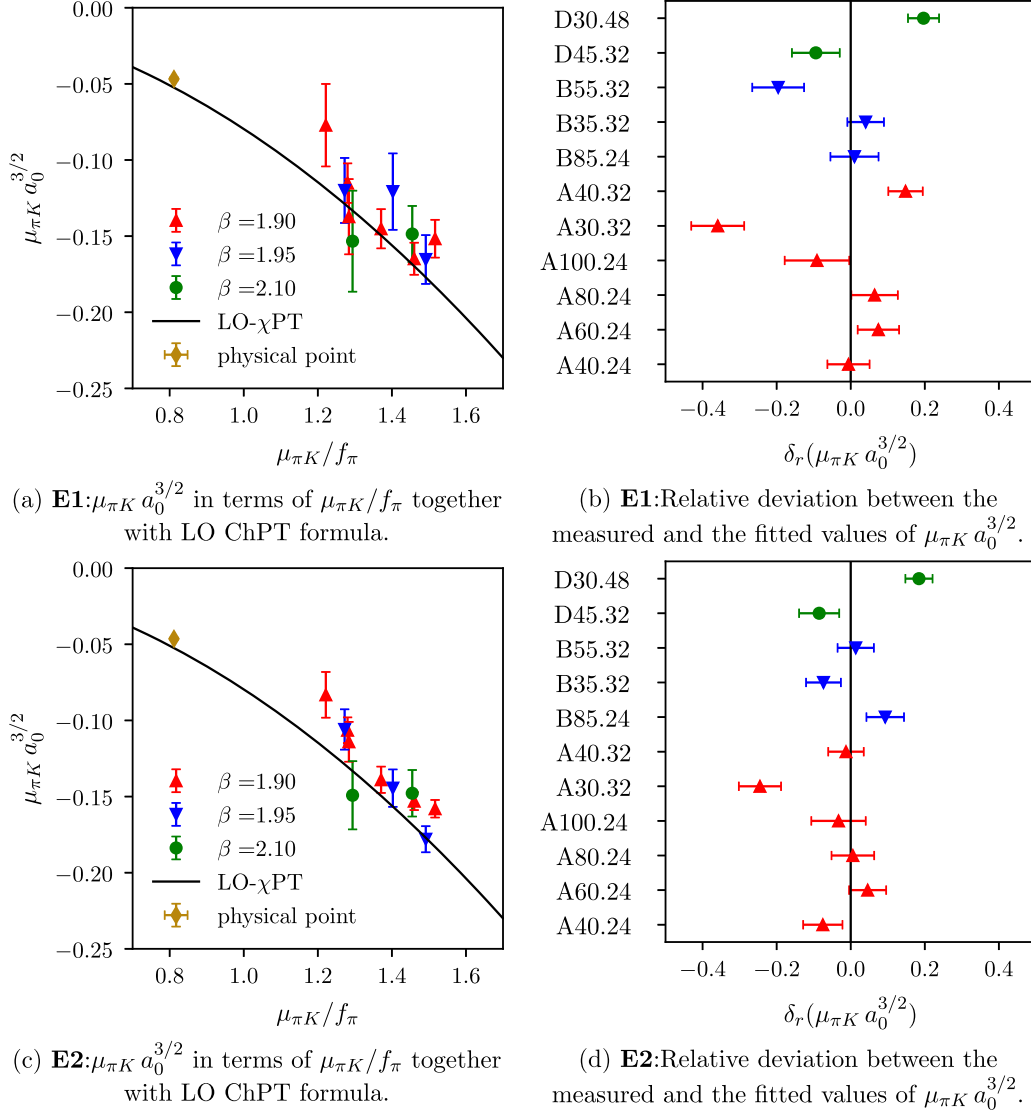
FIG. 4.   Chiral extrapolation of $\mu_{\pi K} a_0^{3/2}$ for **E1** and **E2**. Different colors and symbols denote different values of β. In black, we plot the LO ChPT formula. The golden diamond gives our final result using the given method at the physical point.

choices of $f(a^2)$. We are neither able to obtain a statistically significant result for the fit parameter c, nor do we see significant differences in the extracted values of $L_{\pi K}$ and $\mu_{\pi K} a_0^{3/2}$. We conclude that within our statistical uncertainties we are not able to resolve lattice artifacts in this quantity. Consequently we are justfied to fit all of our data simultaneously with the continuum ChPT formula Eq. (34) and to claim that at this order in the chiral expansion, our results correspond to the physical point in the continuum limit.

In the right column of the plots in Fig. 4, we show the lattice data for $\mu_{\pi K} a_0^{3/2}$ interpolated to the reference strange quark mass as a function of $\mu_{\pi K}/f_\pi$ for the two thermal pollution removal methods **E1** and **E2**. The solid line corresponds to the leading order,

parameter-free ChPT prediction. Plotting our best fit curve with NLO ChPT together with the data is difficult, because $\mu_{\pi K} a_0^{3/2}$ depends on meson masses and f_π besides $\mu_{\pi K}/f_\pi$. Therefore, in order to demonstrate that the fit is able to describe our data, we indicate the relative deviation $\delta_r(\mu_{\pi K} a_0^{3/2})$ between the fitted points and the original data

$$\delta_r(\mu_{\pi K} a_0^{3/2}) = \frac{(\mu_{\pi K} a_0^{3/2})^{\text{meas}} - (\mu_{\pi K} a_0^{3/2})^{\text{fit}}}{(\mu_{\pi K} a_0^{3/2})^{\text{meas}}}, \quad (44)$$

in Figs. 4(b) and 4(d). The indicated error bars are statistical only and it is clear that within these uncertainties, our data is reasonably well described by the fit.

(a) Pollution Removal **E1**   (b) Pollution Removal **E2**
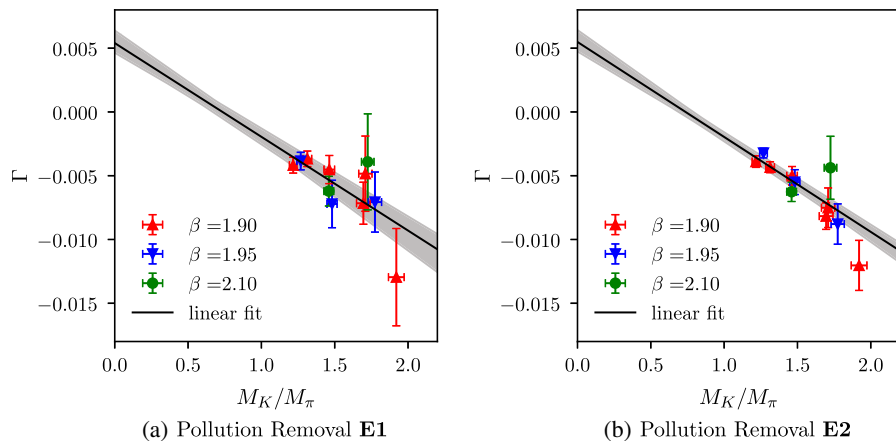
FIG. 5. Chiral extrapolation using the Γ method with data interpolated to the reference strange quark mass. The data for different lattice spacings are color encoded. In addition, we show the linear fit (solid curve, gray error band).

As in Sec. V D 2, to investigate the validity of Eq. (34) across our entire range of pion masses, we studied three different fit intervals for $\mu_{\pi K}/f_\pi$, namely

$$\frac{\mu_{\pi K}}{f_\pi} \in \{(0; 1.35), (0; 1.41), (0; 1.60)\}, \qquad (45)$$

where now the first range corresponds to only using our lightest pion masses and the third range includes all of our ensembles. The resulting trend in the extracted values of $L_{\pi K}$ and $\mu_{\pi K} a_0^{3/2}$ is shown in Table VII. Just as in the study of the Γ-method, including heavier pion masses leads to smaller values of $L_{\pi K}$ and correspondingly smaller values of $\mu_{\pi K} a_0^{3/2}$.

2. Γ Method

In this section, we present results employing the determination of $L_{\pi K}$ using the linear fit introduced in Sec. III E. Figure 5 shows the chiral extrapolations in terms of M_K/M_π for pollution removal **E1** and **E2**. Since we work at fixed strange quark mass, the light quark mass decreases from left to right in the figure. In order to check how our extraction of $L_{\pi K}$ is affected by the range of included pion masses, we employ three different fit ranges

$$\frac{M_K}{M_\pi} \in \{(0; 2.0), (1.5; 2.0), (1.4; 2.0)\}. \qquad (46)$$

In Table V, we compile the results for the fits corresponding to the data points of Fig. 5 for all three fit ranges. As the fit range is restricted to our lightest ensembles, the value extracted for $L_{\pi K}$ tends up, while the absolute value of the extracted $\mu_{\pi K} a_0^{3/2}$ decreases. It is worth noting that this behavior is only observed for the pollution removal **E2**, whereas for **E1** the values for

$L_{\pi K}$ and $\mu_{\pi K} a_0^{3/2}$ stay constant within their statistical errors.

VI. DISCUSSION

Let us first discuss the main systematics of our computation: In contrast to the pion-pion or kaon-kaon systems, there is time dependent thermal pollution in the correlation functions relevant for the extraction of the pion-kaon s-wave scattering length. This very fact turns out to represent one of the major systematic uncertainties in the present computation. We have investigated two methods to remove the leading thermal pollution, denoted as **E1** and **E2**. With both we are able to describe the data for the correlation functions. However, there is uncertainty left, because we remove only the leading pollution and the removal procedure requires input estimated from other two point functions. Thus, we eventually decided to use both methods **E1** and **E2** and include the differences in the systematic uncertainty.

Second, we perform a mixed action simulation for the strange quark. We use this to correct for small mistuning in the sea strange quark mass value used for the gauge configuration generation. This leads—at least in principle—to a small mismatch in the renormalization condition used for the continuum extrapolation. We cannot resolve the corresponding effect on our results quantitatively given our statistical uncertainties. But, since we study quantities which mainly depend on the valence quark properties we expect them to be small.

Third, in the ChPT determination of $L_{\pi K}$ the remaining LEC, L_5, entered as a prior to numerically stabilize our fits. The HPQCD value of Ref. [35] stems from an independent lattice simulation, but is extrapolated to the continuum limit. In Ref. [35], L_5 is given at scale M_η, which we translated to our renormalization scale given by the pion decay constant.
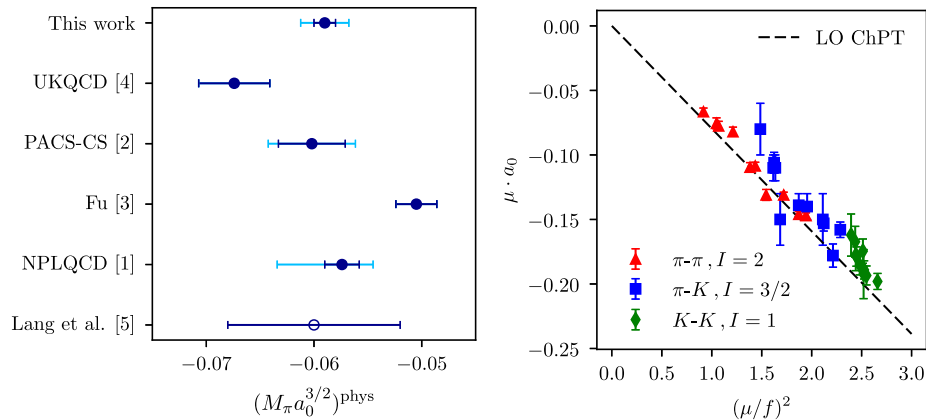
FIG. 6.   Left: Comparison of physical results for $M_\pi a_0^{I=3/2}$ from various lattice computations [1–5]. The unfilled point denotes the LO extrapolation to the physical point using the data of Ref. [5]. Right: s-wave scattering lengths for the pion-pion, pion-kaon and kaon-kaon maximum isospin channels as a function of the squared reduced mass μ^2 of the system divided by f_π^2 for pion-pion and pion-kaon and by f_K^2 for kaon-kaon.

In addition, the extrapolation from our data to the physical point is quite long. Here, a computation directly with physical pion mass would improve our confidence in the result. The final error on our determination is only as small as it is due to the highly constraining ChPT description of $\mu_{\pi K} a_0^{3/2}$.

Finally, although we are not able to resolve lattice artifacts in our determination of $\mu_{\pi K} a_0^{3/2}$ our statistical errors and limited set of gauge ensembles especially at the finest lattice spacing might make us unable to resolve possible lattice artifacts.

VII. SUMMARY

In this paper, we have presented a first lattice computation of the pion-kaon s-wave scattering length for isospin $I = 3/2$ extrapolated to the continuum limit. By varying our methodology we estimate the systematic uncertainties in our results. Our errors cover statistical uncertainties, continuum and chiral extrapolations as well as the removal of thermal pollution.

In the left panel of Fig. 6, we compare the results presented in this paper with previous lattice determinations. The inner (darker) error bars show the purely statistical errors whereas the outer (lighter) ones correspond to the statistical and systematic errors added in quadrature. Even though the four other determinations lack the extrapolation to the continuum limit, overall agreement within errors is observed. However, concerning the final uncertainty, our determination improves significantly on the previous determinations by controlling more sources of uncertainty.

As mentioned in the introduction, the three two particle systems pion-pion, pion-kaon and kaon-kaon are very similar. Therefore, it is interesting to compare the data for pion-pion [9], kaon-kaon [11] and pion-kaon in a single

plot. This is done in the right panel of Fig. 6 where we show $\mu \cdot a_0$ as a function of $(\mu/f)^2$. Here μ is the reduced mass of the corresponding two particle system and f is the pion decay constant f_π for the pion-pion and pion-kaon and f_K for the kaon-kaon system. The dashed line in the right panel of Fig. 6 is the leading-order, parameter-free ChPT prediction all three systems share. The three symbols (and colors) represent our data for the three different systems, respectively.

It can be seen that for all three systems, the deviations from LO ChPT are small. For the pion-kaon system, a parametrization in terms of $f_K \cdot f_\pi$ would bring the points even closer to the LO line, while increasing the deviation of the final result from the LO estimate. For the kaon-kaon system, instead, a parametrization in terms of f_π rather than f_K (which is perfectly valid at this order of ChPT) would render the deviation from the LO line more severe.

It is somewhat surprising that ChPT appears to work so well for all three systems, especially for the heavier points in our simulations and even more for the kaon-kaon system, where the expansion parameter becomes large. A possible reason for this finding might be the fact that all three systems are only weakly interacting.

[37], QUDA [38–40], R [41], PYTHON [42] and SCIPY [43] have been used.

APPENDIX A: π-K SCATTERING IN ChPT

1. Isospin even/odd scattering amplitudes

For completeness, we reproduce here the derivation of the Γ method [1] described in Sec. III E. The scattering amplitudes for all isospin channels of π-K scattering can be noted down using basis elements that are even (odd) under exchange of the Mandelstam variables s and u

$$\mathcal{A}^+ = \frac{1}{3}(\mathcal{A}^{1/2}(s,t,u) + 2\mathcal{A}^{3/2}(s,t,u))$$
$$\mathcal{A}^- = \frac{1}{3}(\mathcal{A}^{1/2}(s,t,u) - \mathcal{A}^{3/2}(s,t,u)). \quad (A1)$$

From Eq. (A1), it follows that

$$\mathcal{A}^{1/2} = \mathcal{A}^+ + 2\mathcal{A}^- \quad (A2)$$

$$\mathcal{A}^{3/2} = \mathcal{A}^+ - \mathcal{A}^-, \quad (A3)$$

which immediately carries over to the scattering lengths $a^{1/2}$ and $a^{3/2}$ yielding

$$\mu_{\pi K} a_0^{1/2} = \mu_{\pi K}(a^+ + 2a^-) \quad (A4)$$

$$\mu_{\pi K} a_0^{3/2} = \mu_{\pi K}(a^+ - a^-). \quad (A5)$$

The scattering lengths a^+ and a^- can be derived from the amplitudes of Eq. (A1), as was done in Ref. [30]. For convenience, we reproduce them here,

$$a^- = \frac{\mu_{\pi K}}{8\pi f_\pi^2}\left\{1 + \frac{M_\pi^2}{f_\pi^2}\left[8L_5 - \frac{1}{2}\chi_{\mathrm{NLO}}^-(\Lambda_\chi, M_\pi, M_K, M_\eta)\right]\right\} \quad (A6)$$

$$a^+ = \frac{\mu_{\pi K} M_K M_\pi}{8\pi f_\pi^4}[16L_{\pi K} + \chi_{\mathrm{NLO}}^+(\Lambda_\chi, M_\pi, M_K, M_\eta)], \quad (A7)$$

with the renormalization scale Λ_χ and the abbreviations $\chi^\pm(\Lambda_\chi, M_\pi, M_K, M_\eta)$ denoted in Appendix A 2. Please note that a^+ only depends on L_5 while a^- only depends on $L_{\pi K}$. Inserting the ChPT formulae for a^+ and a^- into Eq. (A4) one arrives at Eq. (36).

2. Next-to-leading-order functions

For convenience, we list the chiral functions $\chi_{\mathrm{NLO}}^\pm$ derived in Ref. [30],

$$\chi_{\mathrm{NLO}}^+(\Lambda_\chi, M_\pi, M_K, M_\eta)$$
$$= \frac{1}{16\pi^2}\left[\nu_\pi \ln\frac{M_\pi}{\Lambda_\chi} + \nu_K \ln\frac{M_K}{\Lambda_\chi} + \nu_\eta \ln\frac{M_\eta}{\Lambda_\chi}\right.$$
$$+ \nu_{\tan} \arctan\left(\frac{2(M_K + M_\pi)}{M_K - 2M_\pi}\sqrt{\frac{M_K - M_\pi}{2M_K + M_\pi}}\right)$$
$$\left.+ \nu\prime_{\tan} \arctan\left(\frac{2(M_K - M_\pi)}{M_K + 2M_\pi}\sqrt{\frac{M_K + M_\pi}{2M_K - M_\pi}}\right) + \frac{43}{9}\right], \quad (A8)$$

$$\chi_{\mathrm{NLO}}^-(\Lambda_\chi, M_\pi, M_K, M_\eta)$$
$$= \frac{M_\pi^2}{8f_\pi^2\pi^2}\left[\nu\prime_\pi \ln\frac{M_\pi}{\Lambda_\chi} + \nu\prime_K \ln\frac{M_K}{\Lambda_\chi} + \nu\prime_\eta \ln\frac{M_\eta}{\Lambda_\chi}\right.$$
$$\left.+ \frac{M_K}{M_\pi}\nu\prime_{\tan} \arctan\left(\frac{2(M_K - M_\pi)}{M_K + 2M_\pi}\sqrt{\frac{M_K + M_\pi}{2M_K - M_\pi}}\right)\right]. \quad (A9)$$

The functions $\nu_X^{(\prime)}$ are given by

$$\nu_\pi = \frac{11M_\pi^2}{2(M_K^2 - M_\pi^2)} \quad (A10)$$

$$\nu_K = -\frac{67M_K^2 - 8M_\pi^2}{9(M_K^2 - M_\pi^2)} \quad (A11)$$

$$\nu_\eta = +\frac{24M_K^2 - 5M_\pi^2}{18(M_K^2 - M_\pi^2)} \quad (A12)$$

$$\nu_{\tan} = -\frac{4}{9}\frac{\sqrt{2M_K^2 - M_K M_\pi - M_\pi^2}}{M_K + M_\pi} \quad (A13)$$

$$\nu\prime_\pi = -\frac{8M_\pi^2 - 5M_\pi^2}{2(M_K^2 - M_\pi^2)} \quad (A14)$$

$$\nu\prime_K = \frac{23M_K^2}{9(M_K^2 - M_\pi^2)} \quad (A15)$$

$$\nu\prime_\eta = \frac{28M_K^2 - 9M_\pi^2}{18(M_K^2 - M_\pi^2)} \quad (A16)$$

$$\nu\prime_{\tan} = -\frac{4}{9}\frac{\sqrt{2M_K^2 - M_K M_\pi - M_\pi^2}}{M_K + M_\pi}. \quad (A17)$$

From these isospin even/odd functions the definite isospin functions $\chi_{\mathrm{NLO}}^{3/2}$ and $\chi_{\mathrm{NLO}}^{1/2}$ can be derived in the same way as the scattering lengths of Eqs. (A4) and (A5),

$$\chi_{\mathrm{NLO}}^{3/2}(\Lambda_\chi, M_\pi, M_K) = \kappa_\pi \ln\frac{M_\pi^2}{\Lambda_\chi^2} + \kappa_K \ln\frac{M_K^2}{\Lambda_\chi^2} + \kappa_\eta \ln\frac{M_\eta^2}{\Lambda_\chi^2} + \frac{86}{9} M_K M_\pi + \kappa_{\tan} \arctan\left(\frac{2(M_K - M_\pi)}{M_K + 2M_\pi}\sqrt{\frac{M_K + M_\pi}{2M_K - M_\pi}}\right),$$

$$\chi_{\mathrm{NLO}}^{1/2}(\Lambda_\chi, M_\pi, M_K) = \kappa_\pi' \ln\frac{M_\pi^2}{\Lambda_\chi^2} + \kappa_K' \ln\frac{M_K^2}{\Lambda_\chi^2} + \kappa_\eta' \ln\frac{M_\eta^2}{\Lambda_\chi^2} + \frac{86}{9} M_K M_\pi + \frac{3}{2}\kappa_{\tan} \arctan\left(\frac{2(M_K - M_\pi)}{M_K + 2M_\pi}\sqrt{\frac{M_K + M_\pi}{2M_K - M_\pi}}\right)$$

$$+ \kappa_{\tan}' \arctan\left(\frac{2(M_K + M_\pi)}{M_K - 2M_\pi}\sqrt{\frac{M_K - M_\pi}{2M_K + M_\pi}}\right) + \kappa_{\tan}' \arctan\left(\frac{2(M_K + M_\pi)}{M_K - 2M_\pi}\sqrt{\frac{M_K - M_\pi}{2M_K + M_\pi}}\right). \quad \text{(A18)}$$

Here the functions $\kappa_X^{(\prime)}$ are given by

$$\kappa_\pi = \frac{11M_K M_\pi^3 + 8M_\pi^2 M_K^2 - 5M_\pi^4}{2(M_K^2 - M_\pi^2)} \quad \text{(A19)}$$

$$\kappa_K = -\frac{67M_K^3 M_\pi - 8M_\pi^3 M_K + 23M_K^2 M_\pi^2}{9(M_K^2 - M_\pi^2)} \quad \text{(A20)}$$

$$\kappa_\eta = \frac{24M_\pi M_K^3 - 5M_K M_\pi^3 + 28M_K^2 M_\pi^2 - 9M_\pi^4}{18(M_K^2 - M_\pi^2)} \quad \text{(A21)}$$

$$\kappa_{\tan} = -\frac{16M_K M_\pi}{9}\frac{\sqrt{2M_K^2 + M_K M_\pi - M_\pi^2}}{M_K - M_\pi} \quad \text{(A22)}$$

$$\kappa_\pi' = \frac{11M_K M_\pi^3 - 16M_K^2 M_\pi^2 + 10M_\pi^4}{2(M_K^2 - M_\pi^2)} \quad \text{(A23)}$$

$$\kappa_K' = -\frac{67M_K^3 M_\pi - 8M_\pi^3 M_K - 46M_K^2 M_\pi^2}{9(M_K^2 - M_\pi^2)} \quad \text{(A24)}$$

$$\kappa_\eta' = \frac{24M_\pi M_K^3 - 5M_K M_\pi^3 - 56M_K^2 M_\pi^2 + 18M_\pi^4}{18(M_K^2 - M_\pi^2)} \quad \text{(A25)}$$

$$\kappa_{\tan}' = \frac{8M_K M_\pi}{9}\frac{\sqrt{2M_K^2 - M_K M_\pi - M_\pi^2}}{M_K + M_\pi}. \quad \text{(A26)}$$

APPENDIX B: DATA TABLES

1. Interpolated data

TABLE IX. Physical values of the scattering length and $L_{\pi K}$ after averaging over the fit ranges.

ChPT	$E_{\pi K}$	$\mu_{\pi K} a_0^{3/2} \times 10^2$	$L_{\pi K} \times 10^3$	$\mu_{\pi K} a_0^{1/2}$	$M_\pi a_0^{3/2} \times 10^2$	$M_\pi a_0^{1/2}$
Γ	**E1**	−4.7(1)	3.7(2)	0.128(2)	−6.0(1)	0.162(2)
	E2	−4.59(8)	3.8(1)	0.129(2)	−5.8(1)	0.164(2)
NLO	**E1**	−4.7(1)	3.6(2)	0.127(2)	−6.0(1)	0.162(2)
	E2	−4.61(9)	3.8(2)	0.129(2)	−5.9(1)	0.164(2)

TABLE X. Comparison of $E_{\pi K}$ for methods **E1** and **E2**.

Ensemble	$a\mu_s$	$aE_{\pi K}(\mathbf{E1})$	$aE_{\pi K}(\mathbf{E2})$
A30.32	0.0185	$0.3558(9)\binom{+7}{-2}$	$0.3558(7)\binom{+5}{-1}$
	0.0225	$0.3758(9)\binom{+8}{-2}$	$0.3758(7)\binom{+6}{-1}$
	0.0246	$0.3870(9)\binom{+9}{-5}$	$0.3867(6)\binom{+2}{-2}$
A40.24	0.0185	$0.3892(12)\binom{+6}{-0}$	$0.3887(11)\binom{+4}{-2}$
	0.0225	$0.4081(12)\binom{+10}{-2}$	$0.4082(11)\binom{+5}{-0}$
	0.0246	$0.4184(12)\binom{+7}{-0}$	$0.4182(11)\binom{+5}{-0}$
A40.32	0.0185	$0.3793(6)\binom{+3}{-8}$	$0.3789(5)\binom{+0}{-4}$
	0.0225	$0.3988(6)\binom{+9}{-7}$	$0.3983(5)\binom{+1}{-3}$
	0.0246	$0.4081(6)\binom{+2}{-4}$	$0.4083(5)\binom{+1}{-4}$
A60.24	0.0185	$0.4250(9)\binom{+11}{-0}$	$0.4247(7)\binom{+8}{-0}$
	0.0225	$0.4447(7)\binom{+2}{-0}$	$0.4440(6)\binom{+3}{-4}$
	0.0246	$0.4537(7)\binom{+8}{-4}$	$0.4536(6)\binom{+5}{-1}$
A80.24	0.0185	$0.4613(6)\binom{+0}{-2}$	$0.4606(5)\binom{+3}{-0}$
	0.0225	$0.4789(6)\binom{+5}{-0}$	$0.4787(5)\binom{+4}{-0}$
	0.0246	$0.4894(6)\binom{+0}{-6}$	$0.4882(5)\binom{+3}{-0}$
A100.24	0.0185	$0.4921(5)\binom{+6}{-3}$	$0.4922(4)\binom{+3}{-0}$
	0.0225	$0.5102(5)\binom{+5}{-0}$	$0.5102(4)\binom{+3}{-0}$
	0.0246	$0.5193(5)\binom{+3}{-3}$	$0.5193(4)\binom{+2}{-1}$
B35.32	0.0160	$0.3333(9)\binom{+11}{-0}$	$0.3336(6)\binom{+6}{-0}$
	0.0186	$0.3474(7)\binom{+2}{-1}$	$0.3472(6)\binom{+3}{-1}$
	0.0210	$0.3595(9)\binom{+0}{-3}$	$0.3584(7)\binom{+5}{-0}$
B55.32	0.0160	$0.3743(5)\binom{+4}{-1}$	$0.3747(4)\binom{+3}{-0}$
	0.0186	$0.3866(5)\binom{+6}{-7}$	$0.3869(4)\binom{+3}{-1}$
	0.0210	$0.3977(5)\binom{+4}{-1}$	$0.3981(4)\binom{+3}{-0}$
B85.24	0.0160	$0.4322(7)\binom{+15}{-2}$	$0.4325(6)\binom{+7}{-0}$
	0.0186	$0.4442(7)\binom{+15}{-1}$	$0.4441(6)\binom{+8}{-1}$
	0.0210	$0.4548(7)\binom{+13}{-0}$	$0.4544(6)\binom{+8}{-1}$
D45.32	0.0130	$0.2925(12)\binom{+23}{-0}$	$0.2922(9)\binom{+18}{-0}$
	0.0150	$0.3028(11)\binom{+5}{-1}$	$0.3010(9)\binom{+14}{-0}$
	0.0180	$0.3145(10)\binom{+16}{-0}$	$0.3142(8)\binom{+12}{-0}$
D30.48	0.0115	$0.2506(8)\binom{+3}{-5}$	$0.2508(5)\binom{+1}{-5}$
	0.0150	$0.2677(8)\binom{+3}{-6}$	$0.2679(6)\binom{+1}{-6}$
	0.0180	$0.2811(8)\binom{+3}{-6}$	$0.2814(6)\binom{+1}{-7}$

TABLE XI.   Comparison of the meson masses, M_π and M_K together with the reduced mass $\mu_{\pi K}$. The systematic uncertainties for $\mu_{\pi K}$ turn out to be negligible and thus are not shown.

Ensemble	$a\mu_s$	aM_K	aM_π	$a\mu_{\pi K}$
A30.32	0.0185	$0.2294(3)\binom{+0}{-0}$	$0.1239(2)\binom{+1}{-0}$	$0.08046(12)\binom{+0}{-0}$
	0.0225	$0.2495(2)\binom{+1}{-0}$	$0.1239(2)\binom{+1}{-0}$	$0.08280(12)\binom{+0}{-0}$
	0.0246	$0.2597(2)\binom{+1}{-0}$	$0.1239(2)\binom{+1}{-0}$	$0.08388(12)\binom{+0}{-0}$
A40.24	0.0185	$0.2365(5)\binom{+2}{-1}$	$0.1453(5)\binom{+2}{-1}$	$0.08999(22)\binom{+0}{-0}$
	0.0225	$0.2561(4)\binom{+4}{-1}$	$0.1453(5)\binom{+2}{-1}$	$0.09269(22)\binom{+0}{-0}$
	0.0246	$0.2662(5)\binom{+1}{-2}$	$0.1453(5)\binom{+2}{-1}$	$0.09398(22)\binom{+0}{-0}$
A40.32	0.0185	$0.2343(2)\binom{+0}{-0}$	$0.1415(2)\binom{+1}{-0}$	$0.08822(10)\binom{+0}{-0}$
	0.0225	$0.2538(2)\binom{+1}{-0}$	$0.1415(2)\binom{+1}{-0}$	$0.09086(11)\binom{+0}{-0}$
	0.0246	$0.2638(2)\binom{+1}{-1}$	$0.1415(2)\binom{+1}{-0}$	$0.09210(11)\binom{+0}{-0}$
A60.24	0.0185	$0.2448(3)\binom{+1}{-0}$	$0.1729(3)\binom{+4}{-1}$	$0.10134(16)\binom{+0}{-0}$
	0.0225	$0.2637(3)\binom{+1}{-0}$	$0.1729(3)\binom{+4}{-1}$	$0.10445(16)\binom{+0}{-0}$
	0.0246	$0.2735(3)\binom{+1}{-0}$	$0.1729(3)\binom{+4}{-1}$	$0.10594(17)\binom{+0}{-0}$
A80.24	0.0185	$0.2548(2)\binom{+0}{-1}$	$0.1993(2)\binom{+0}{-1}$	$0.11184(11)\binom{+0}{-0}$
	0.0225	$0.2731(2)\binom{+1}{-1}$	$0.1993(2)\binom{+0}{-1}$	$0.11523(11)\binom{+0}{-0}$
	0.0246	$0.2824(2)\binom{+2}{-2}$	$0.1993(2)\binom{+0}{-1}$	$0.11685(11)\binom{+0}{-0}$
A100.24	0.0185	$0.2642(2)\binom{+0}{-1}$	$0.2223(2)\binom{+1}{-1}$	$0.12073(11)\binom{+0}{-0}$
	0.0225	$0.2822(2)\binom{+0}{-0}$	$0.2223(2)\binom{+1}{-1}$	$0.12436(11)\binom{+0}{-0}$
	0.0246	$0.2913(2)\binom{+1}{-1}$	$0.2223(2)\binom{+1}{-1}$	$0.12609(11)\binom{+0}{-0}$
B35.32	0.0160	$0.2053(2)\binom{+1}{-1}$	$0.1249(2)\binom{+1}{-1}$	$0.07765(11)\binom{+0}{-0}$
	0.0186	$0.2186(2)\binom{+2}{-1}$	$0.1249(2)\binom{+1}{-1}$	$0.07948(12)\binom{+0}{-0}$
	0.0210	$0.2298(2)\binom{+0}{-1}$	$0.1249(2)\binom{+1}{-1}$	$0.08091(12)\binom{+0}{-0}$
B55.32	0.0160	$0.2155(2)\binom{+1}{-2}$	$0.1554(2)\binom{+0}{-0}$	$0.09030(10)\binom{+0}{-0}$
	0.0186	$0.2282(2)\binom{+1}{-2}$	$0.1554(2)\binom{+0}{-0}$	$0.09245(10)\binom{+0}{-0}$
	0.0210	$0.2390(2)\binom{+1}{-2}$	$0.1554(2)\binom{+0}{-0}$	$0.09418(10)\binom{+0}{-0}$
B85.24	0.0160	$0.2313(3)\binom{+0}{-3}$	$0.1933(3)\binom{+1}{-0}$	$0.10530(15)\binom{+0}{-0}$
	0.0186	$0.2429(3)\binom{+0}{-0}$	$0.1933(3)\binom{+1}{-0}$	$0.10763(16)\binom{+0}{-0}$
	0.0210	$0.2535(3)\binom{+2}{-0}$	$0.1933(3)\binom{+1}{-0}$	$0.10967(15)\binom{+0}{-0}$
D45.32	0.0130	$0.1658(3)\binom{+1}{-1}$	$0.1205(4)\binom{+1}{-1}$	$0.06979(17)\binom{+0}{-0}$
	0.0150	$0.1747(4)\binom{+4}{-1}$	$0.1205(4)\binom{+1}{-1}$	$0.07132(17)\binom{+0}{-0}$
	0.0180	$0.1876(3)\binom{+0}{-1}$	$0.1205(4)\binom{+1}{-1}$	$0.07339(17)\binom{+0}{-0}$
D30.48	0.0115	$0.1503(1)\binom{+0}{-0}$	$0.0976(1)\binom{+0}{-0}$	$0.05917(6)\binom{+0}{-0}$
	0.0150	$0.1673(1)\binom{+0}{-1}$	$0.0976(1)\binom{+0}{-0}$	$0.06163(6)\binom{+0}{-0}$
	0.0180	$0.1807(1)\binom{+1}{-1}$	$0.0976(1)\binom{+0}{-0}$	$0.06336(6)\binom{+0}{-0}$

TABLE XII. Comparison of $\delta E_{\pi K}$ for methods **E1** and **E2**.

Ensemble	$a\mu_s$	$a\delta E(\mathbf{E1}) \times 10^3$	$a\delta E(\mathbf{E2}) \times 10^3$
A30.32	0.0185	$2.48(96)\binom{+68}{-20}$	$2.44(81)\binom{+51}{-8}$
	0.0225	$2.41(97)\binom{+81}{-17}$	$2.34(77)\binom{+57}{-8}$
	0.0246	$3.45(93)\binom{+89}{-49}$	$3.14(74)\binom{+19}{-22}$
A40.24	0.0185	$7.46(84)\binom{+56}{-0}$	$6.93(56)\binom{+43}{-20}$
	0.0225	$6.70(85)\binom{+97}{-19}$	$6.84(67)\binom{+47}{-1}$
	0.0246	$6.94(88)\binom{+74}{-0}$	$6.69(61)\binom{+50}{-1}$
A40.32	0.0185	$3.52(47)\binom{+34}{-83}$	$3.15(32)\binom{+0}{-38}$
	0.0225	$3.42(45)\binom{+85}{-73}$	$2.96(29)\binom{+8}{-27}$
	0.0246	$2.79(44)\binom{+15}{-42}$	$2.99(31)\binom{+13}{-39}$
A60.24	0.0185	$7.25(69)\binom{+111}{-0}$	$7.02(39)\binom{+80}{-0}$
	0.0225	$8.05(46)\binom{+24}{-3}$	$7.37(35)\binom{+34}{-36}$
	0.0246	$7.28(45)\binom{+78}{-43}$	$7.22(30)\binom{+46}{-12}$
A80.24	0.0185	$7.19(48)\binom{+3}{-22}$	$6.45(21)\binom{+30}{-0}$
	0.0225	$6.47(47)\binom{+48}{-0}$	$6.19(23)\binom{+39}{-0}$
	0.0246	$7.61(48)\binom{+0}{-57}$	$6.40(21)\binom{+34}{-0}$
A100.24	0.0185	$5.58(32)\binom{+61}{-30}$	$5.70(17)\binom{+27}{-3}$
	0.0225	$5.68(32)\binom{+48}{-0}$	$5.67(17)\binom{+26}{-0}$
	0.0246	$5.74(24)\binom{+34}{-30}$	$5.69(14)\binom{+19}{-7}$
B35.32	0.0160	$3.12(85)\binom{+109}{-0}$	$3.38(45)\binom{+62}{-0}$
	0.0186	$3.94(54)\binom{+23}{-8}$	$3.67(34)\binom{+30}{-13}$
	0.0210	$4.79(85)\binom{+0}{-33}$	$3.72(56)\binom{+53}{-0}$
B55.32	0.0160	$3.33(42)\binom{+44}{-12}$	$3.71(30)\binom{+28}{-2}$
	0.0186	$3.02(45)\binom{+64}{-74}$	$3.27(33)\binom{+30}{-8}$
	0.0210	$3.28(41)\binom{+43}{-12}$	$3.65(30)\binom{+27}{-1}$
B85.24	0.0160	$7.61(41)\binom{+153}{-16}$	$7.88(23)\binom{+66}{-0}$
	0.0186	$8.05(36)\binom{+150}{-14}$	$7.97(23)\binom{+81}{-5}$
	0.0210	$7.99(38)\binom{+127}{-3}$	$7.64(25)\binom{+81}{-9}$
D45.32	0.0130	$6.18(88)\binom{+232}{-0}$	$5.87(53)\binom{+177}{-0}$
	0.0150	$7.62(86)\binom{+54}{-12}$	$5.82(43)\binom{+143}{-0}$
	0.0180	$6.38(71)\binom{+158}{-0}$	$6.05(45)\binom{+120}{-0}$
D30.48	0.0115	$2.70(77)\binom{+26}{-53}$	$2.90(50)\binom{+10}{-53}$
	0.0150	$2.79(79)\binom{+26}{-60}$	$3.05(51)\binom{+9}{-63}$
	0.0180	$2.86(82)\binom{+25}{-65}$	$3.17(54)\binom{+9}{-69}$

TABLE XIII. External data used via parametric bootstrapping. The error on $K_{M_K}^{\mathrm{FSE}}$ is only estimated.

Ensemble	f_π	$K_{f_\pi}^{\mathrm{FSE}}$	$K_{M_\pi}^{\mathrm{FSE}}$	$K_{M_K}^{\mathrm{FSE}}$
A30.32	0.064 52(21)	0.9757(61)	1.0081(52)	1.002 327(1)
A40.24	0.065 77(24)	0.9406(84)	1.0206(95)	1.009 874(1)
A40.32	0.068 39(18)	0.9874(24)	1.0039(28)	1.001 299(1)
A60.24	0.072 09(20)	0.9716(37)	1.0099(49)	1.004 681(1)
A80.24	0.075 81(13)	0.9839(22)	1.0057(29)	1.002 518(1)
A100.24	0.079 36(14)	0.9900(15)	1.0037(19)	1.001 480(1)
B35.32	0.061 05(17)	0.9794(27)	1.0069(32)	1.002 466(1)
B55.32	0.065 45(11)	0.9920(10)	1.0027(14)	1.000 879(1)
B85.24	0.070 39(26)	0.9795(24)	1.0083(28)	1.003 178(1)
D30.48	0.047 35(15)	0.9938(5)	1.0021(7)	1.000 714(1)
D45.32	0.048 25(14)	0.9860(13)	1.0047(14)	1.000 000(1)

TABLE XIV. Comparison of a_0 and $\mu_{\pi K}a_0^{3/2}$ for methods **E1** and **E2**.

Ensemble	$a\mu_s$	a_0/a(**E1**)	a_0/a(**E2**)	$\mu_{\pi K}a_0^{3/2}$(**E1**)	$\mu_{\pi K}a_0^{3/2}$(**E2**)
A30.32	0.0185	$-0.96(34)\left(^{+7}_{-24}\right)$	$-0.94(29)\left(^{+3}_{-18}\right)$	$-0.077(27)\left(^{+6}_{-19}\right)$	$-0.076(23)\left(^{+2}_{-14}\right)$
	0.0225	$-0.95(35)\left(^{+6}_{-29}\right)$	$-0.93(28)\left(^{+3}_{-20}\right)$	$-0.079(29)\left(^{+5}_{-24}\right)$	$-0.077(23)\left(^{+2}_{-17}\right)$
	0.0246	$-1.33(32)\left(^{+17}_{-30}\right)$	$-1.23(26)\left(^{+8}_{-7}\right)$	$-0.112(27)\left(^{+14}_{-25}\right)$	$-0.103(22)\left(^{+6}_{-6}\right)$
A40.24	0.0185	$-1.27(12)\left(^{+0}_{-8}\right)$	$-1.19(8)\left(^{+3}_{-6}\right)$	$-0.114(11)\left(^{+0}_{-7}\right)$	$-0.107(8)\left(^{+3}_{-6}\right)$
	0.0225	$-1.18(13)\left(^{+3}_{-15}\right)$	$-1.20(10)\left(^{+0}_{-7}\right)$	$-0.110(12)\left(^{+3}_{-14}\right)$	$-0.112(9)\left(^{+0}_{-7}\right)$
	0.0246	$-1.23(14)\left(^{+0}_{-11}\right)$	$-1.20(10)\left(^{+0}_{-8}\right)$	$-0.116(13)\left(^{+0}_{-11}\right)$	$-0.112(9)\left(^{+0}_{-7}\right)$
A40.32	0.0185	$-1.42(17)\left(^{+31}_{-12}\right)$	$-1.29(12)\left(^{+14}_{-0}\right)$	$-0.126(15)\left(^{+27}_{-11}\right)$	$-0.114(10)\left(^{+12}_{-0}\right)$
	0.0225	$-1.42(17)\left(^{+27}_{-31}\right)$	$-1.25(11)\left(^{+10}_{-3}\right)$	$-0.129(15)\left(^{+25}_{-28}\right)$	$-0.114(10)\left(^{+9}_{-3}\right)$
	0.0246	$-1.20(17)\left(^{+17}_{-6}\right)$	$-1.28(12)\left(^{+15}_{-5}\right)$	$-0.111(16)\left(^{+15}_{-5}\right)$	$-0.118(11)\left(^{+14}_{-5}\right)$
A60.24	0.0185	$-1.37(11)\left(^{+0}_{-18}\right)$	$-1.33(6)\left(^{+0}_{-13}\right)$	$-0.139(11)\left(^{+0}_{-18}\right)$	$-0.135(6)\left(^{+0}_{-13}\right)$
	0.0225	$-1.53(7)\left(^{+1}_{-4}\right)$	$-1.42(6)\left(^{+6}_{-6}\right)$	$-0.160(8)\left(^{+1}_{-4}\right)$	$-0.149(6)\left(^{+6}_{-6}\right)$
	0.0246	$-1.43(7)\left(^{+7}_{-13}\right)$	$-1.41(5)\left(^{+2}_{-8}\right)$	$-0.151(8)\left(^{+8}_{-13}\right)$	$-0.150(5)\left(^{+2}_{-8}\right)$
A80.24	0.0185	$-1.48(8)\left(^{+4}_{-1}\right)$	$-1.35(4)\left(^{+0}_{-5}\right)$	$-0.165(9)\left(^{+4}_{-1}\right)$	$-0.150(4)\left(^{+0}_{-6}\right)$
	0.0225	$-1.39(9)\left(^{+0}_{-9}\right)$	$-1.33(4)\left(^{+0}_{-7}\right)$	$-0.160(10)\left(^{+0}_{-10}\right)$	$-0.154(5)\left(^{+0}_{-8}\right)$
	0.0246	$-1.61(8)\left(^{+10}_{-0}\right)$	$-1.39(4)\left(^{+0}_{-6}\right)$	$-0.188(10)\left(^{+12}_{-0}\right)$	$-0.162(5)\left(^{+0}_{-7}\right)$
A100.24	0.0185	$-1.27(6)\left(^{+6}_{-12}\right)$	$-1.29(3)\left(^{+1}_{-5}\right)$	$-0.153(8)\left(^{+7}_{-14}\right)$	$-0.156(4)\left(^{+1}_{-6}\right)$
	0.0225	$-1.32(6)\left(^{+0}_{-9}\right)$	$-1.32(3)\left(^{+0}_{-5}\right)$	$-0.165(8)\left(^{+0}_{-12}\right)$	$-0.164(4)\left(^{+0}_{-7}\right)$
	0.0246	$-1.35(5)\left(^{+6}_{-7}\right)$	$-1.34(3)\left(^{+1}_{-4}\right)$	$-0.170(6)\left(^{+8}_{-9}\right)$	$-0.169(4)\left(^{+2}_{-5}\right)$
B35.32	0.0160	$-1.14(28)\left(^{+0}_{-35}\right)$	$-1.22(15)\left(^{+0}_{-20}\right)$	$-0.088(22)\left(^{+0}_{-27}\right)$	$-0.095(11)\left(^{+0}_{-15}\right)$
	0.0186	$-1.43(17)\left(^{+3}_{-7}\right)$	$-1.34(11)\left(^{+4}_{-10}\right)$	$-0.114(14)\left(^{+2}_{-6}\right)$	$-0.107(9)\left(^{+3}_{-8}\right)$
	0.0210	$-1.73(26)\left(^{+10}_{-0}\right)$	$-1.38(19)\left(^{+0}_{-17}\right)$	$-0.140(21)\left(^{+8}_{-0}\right)$	$-0.112(15)\left(^{+0}_{-14}\right)$
B55.32	0.0160	$-1.38(15)\left(^{+4}_{-16}\right)$	$-1.52(11)\left(^{+1}_{-10}\right)$	$-0.125(14)\left(^{+4}_{-15}\right)$	$-0.137(10)\left(^{+1}_{-9}\right)$
	0.0186	$-1.29(17)\left(^{+29}_{-24}\right)$	$-1.39(12)\left(^{+3}_{-11}\right)$	$-0.120(16)\left(^{+27}_{-22}\right)$	$-0.128(11)\left(^{+3}_{-10}\right)$
	0.0210	$-1.42(16)\left(^{+5}_{-16}\right)$	$-1.55(11)\left(^{+0}_{-10}\right)$	$-0.133(15)\left(^{+4}_{-15}\right)$	$-0.146(10)\left(^{+0}_{-9}\right)$
B85.24	0.0160	$-1.47(7)\left(^{+3}_{-24}\right)$	$-1.52(4)\left(^{+0}_{-11}\right)$	$-0.155(7)\left(^{+3}_{-26}\right)$	$-0.160(4)\left(^{+0}_{-11}\right)$
	0.0186	$-1.57(6)\left(^{+2}_{-24}\right)$	$-1.56(4)\left(^{+1}_{-13}\right)$	$-0.169(6)\left(^{+3}_{-26}\right)$	$-0.168(4)\left(^{+1}_{-14}\right)$
	0.0210	$-1.59(6)\left(^{+1}_{-21}\right)$	$-1.53(4)\left(^{+2}_{-13}\right)$	$-0.174(7)\left(^{+1}_{-23}\right)$	$-0.167(5)\left(^{+2}_{-15}\right)$
D45.32	0.0130	$-1.89(23)\left(^{+0}_{-57}\right)$	$-1.81(14)\left(^{+0}_{-45}\right)$	$-0.132(16)\left(^{+0}_{-40}\right)$	$-0.126(10)\left(^{+0}_{-31}\right)$
	0.0150	$-2.29(21)\left(^{+3}_{-13}\right)$	$-1.83(12)\left(^{+0}_{-37}\right)$	$-0.163(15)\left(^{+2}_{-9}\right)$	$-0.130(8)\left(^{+0}_{-26}\right)$
	0.0180	$-2.02(19)\left(^{+0}_{-41}\right)$	$-1.94(12)\left(^{+0}_{-32}\right)$	$-0.149(14)\left(^{+0}_{-30}\right)$	$-0.142(9)\left(^{+0}_{-23}\right)$
D30.48	0.0115	$-2.43(60)\left(^{+43}_{-20}\right)$	$-2.58(38)\left(^{+42}_{-8}\right)$	$-0.144(36)\left(^{+25}_{-12}\right)$	$-0.152(23)\left(^{+25}_{-5}\right)$
	0.0150	$-2.59(63)\left(^{+49}_{-20}\right)$	$-2.79(40)\left(^{+50}_{-7}\right)$	$-0.159(39)\left(^{+30}_{-12}\right)$	$-0.172(25)\left(^{+31}_{-4}\right)$
	0.0180	$-2.71(66)\left(^{+54}_{-20}\right)$	$-2.95(42)\left(^{+56}_{-7}\right)$	$-0.171(42)\left(^{+34}_{-13}\right)$	$-0.187(27)\left(^{+36}_{-4}\right)$

TABLE XV.   Input data for the chiral analysis.

Ensemble	$\mu_{\pi K}/f_\pi$	aM_K	aM_η	$\mu_{\pi K}a_0^{3/2}$(**E1**)	$\mu_{\pi K}a_0^{3/2}$(**E2**)
A40.24	1.28(2)	0.241(6)	0.317(6)	−0.12(1)	−0.106(8)
A60.24	1.37(1)	0.251(6)	0.323(6)	−0.15(1)	−0.139(9)
A80.24	1.46(1)	0.260(6)	0.327(5)	−0.16(1)	−0.153(6)
A100.24	1.52(1)	0.269(6)	0.332(4)	−0.15(1)	−0.158(6)
A30.32	1.22(1)	0.236(6)	0.314(9)	−0.08(3)	−0.08(2)
A40.32	1.28(1)	0.241(6)	0.314(9)	−0.14(2)	−0.11(1)
B85.24	1.49(1)	0.243(5)	0.296(5)	−0.17(2)	−0.178(9)
B35.32	1.27(1)	0.220(6)	0.284(8)	−0.12(2)	−0.11(1)
B55.32	1.40(1)	0.230(5)	0.283(5)	−0.12(3)	−0.14(1)
D45.32	1.45(1)	0.175(4)	0.200(4)	−0.15(2)	−0.15(2)
D30.48	1.29(1)	0.168(4)	0.196(4)	−0.15(3)	−0.15(2)

[1] S. R. Beane, P. F. Bedaque, T. C. Luu, K. Orginos, E. Pallante, A. Parreño, and M. J. Savage (NPLQCD Collaboration), Phys. Rev. D **74,** 114503 (2006).

[2] K. Sasaki, N. Ishizuka, M. Oka, and T. Yamazaki (PACS-CS Collaboration), Phys. Rev. D **89,** 054502 (2014).

[3] Z. Fu, Phys. Rev. D **85,** 074501 (2012).

[4] T. Janowski, P. A. Boyle, A. Jüttner, and C. Sachrajda, Proc. Sci., LATTICE2014 (**2014**) 080.

[5] C. B. Lang, L. Leskovec, D. Mohler, and S. Prelovsek, Phys. Rev. D **86,** 054508 (2012).

[6] J.-W. Chen, D. O'Connell, R. Van de Water, and A. Walker-Loud, Phys. Rev. D **73,** 074510 (2006).

[7] J.-W. Chen, D. O'Connell, and A. Walker-Loud, Phys. Rev. D **75,** 054501 (2007).

[8] R. Baron et al. (ETM Collaboration), Comput. Phys. Commun. **182,** 299 (2011).

[9] C. Helmes, C. Jost, B. Knippschild, L. Liu, C. Urbach, M. Ueding, M. Werner, C. Liu, J. Liu, and Z. Wang (ETM Collaboration), J. High Energy Phys. 09 (2015) 109.

[10] L. Liu et al., Phys. Rev. D **96,** 054516 (2017).

[11] C. Helmes, C. Jost, B. Knippschild, B. Kostrzewa, L. Liu, C. Urbach, and M. Werner (ETM Collaboration), Phys. Rev. D **96,** 034510 (2017).

[12] T. Chiarappa, F. Farchioni, K. Jansen, I. Montvay, E. E. Scholz, L. Scorzato, T. Sudmann, and C. Urbach, Eur. Phys. J. C **50,** 373 (2007).

[13] R. Baron et al. (ETM Collaboration), J. High Energy Phys. 06 (2010) 111.

[14] R. Frezzotti and G. C. Rossi, J. High Energy Phys. 08 (2004) 007.

[15] R. Frezzotti and G. C. Rossi, Nucl. Phys. B, Proc. Suppl. **128,** 193 (2004).

[16] R. Frezzotti and G. C. Rossi, J. High Energy Phys. 10 (2004) 070.

[17] N. Carrasco et al. (ETM Collaboration), Nucl. Phys. **B887,** 19 (2014).

[18] C. Morningstar, J. Bulava, J. Foley, K. J. Juge, D. Lenkner, M. Peardon, and C. H. Wong, Phys. Rev. D **83,** 114505 (2011).

[19] K. Ottnad, C. Urbach, and F. Zimmermann (ETM Collaboration), Nucl. Phys. **B896,** 470 (2015).

[20] C. Jost (to be published).

[21] M. Lüscher, Commun. Math. Phys. **105,** 153 (1986).

[22] J. Gasser and H. Leutwyler, Ann. Phys. (N.Y.) **158,** 142 (1984).

[23] S. Aoki et al., Eur. Phys. J. C **77,** 112 (2017).

[24] M. Tanabashi et al. (Particle Data Group), Phys. Rev. D **98,** 030001 (2018).

[25] C. Patrignani et al. (Particle Data Group), Chin. Phys. C **40,** 100001 (2016).

[26] R. Sommer, Nucl. Phys. **B411,** 839 (1994).

[27] C. Michael, K. Ottnad, and C. Urbach (ETM Collaboration), Phys. Rev. Lett. **111,** 181602 (2013).

[28] J. J. Dudek, R. G. Edwards, and C. E. Thomas, Phys. Rev. D **86,** 034031 (2012).

[29] V. Bernard, N. Kaiser, and U.-G. Meißner, Nucl. Phys. **B357,** 129 (1991).

[30] B. Kubis and U.-G. Meissner, Phys. Lett. B **529,** 69 (2002).

[31] M. I. Buchoff, J.-W. Chen, and A. Walker-Loud, Phys. Rev. D **79,** 074503 (2009).

[32] D. N. Politis and J. P. Romano, J. Am. Stat. Assoc. **89,** 1303 (1994).

[33] U. Wolff (ALPHA Collaboration), Comput. Phys. Commun. **156,** 143 (2004).

[34] K. Ottnad and C. Urbach (ETM Collaboration), Phys. Rev. D **97,** 054508 (2018).

[35] R. J. Dowdall, C. T. H. Davies, G. P. Lepage, and C. McNeile, Phys. Rev. D **88,** 074504 (2013).

[36] K. Jansen and C. Urbach, Comput. Phys. Commun. **180,** 2717 (2009).

[37] A. Deuzeman, S. Reker, and C. Urbach (ETM Collaboration), Comput. Phys. Commun. **183,** 1321 (2012).

[38] M. A. Clark, R. Babich, K. Barros, R. C. Brower, and C. Rebbi, Comput. Phys. Commun. **181,** 1517 (2010).

[39] R. Babich et al., Scaling Lattice QCD beyond 100 GPUs, in SC11 International Conference for High Performance

Computing, Networking, Storage and Analysis Seattle, Washington, 2011 (ACM, New York, 2011).

[40] M. A. Clark *et al.*, arXiv:1612.07873.

[41] R Development Core Team, *R: A Language and Environment for Statistical Computing* (R Foundation for Statistical Computing, Vienna, Austria, 2005).

[42] G. van Rossum and F. L. Drake, *The Python Language Reference Manual* (Network Theory Ltd., 2001).

[43] E. Jones *et al.*, SciPy: Open source scientific tools for Python, 2001–2018, https://www.bibsonomy.org/bibtex/21b37d2cc741af879d7958f2f7c23c420/microcuts.